THE ASTROPHYSICAL JOURNAL, 448:683–704, 1995 August 1

ROSAT ALL-SKY SURVEY OBSERVATIONS OF THE HYADES CLUSTER

ROBERT A. STERN[1]
Solar and Astrophysics Laboratory, Lockheed Palo Alto Research Laboratory, O/91-30, Building 252, 3251 Hanover Street, Palo Alto, CA 94304

AND

JÜRGEN H. M. M. SCHMITT AND PETER T. KAHABKA
Max-Planck-Institut für Extraterrestrische Physik, Postfach 1603, D-85740 Garching, Germany
Received 1994 November 3; accepted 1995 February 27

ABSTRACT

We report the results of a complete X-ray survey of the Hyades cluster region using the *ROSAT* All-Sky Survey (RASS). Our survey covers over 900 deg^2 of the sky. Over 185 optically identified Hyads were detected down to a limiting X-ray luminosity of ≈ 1–2×10^{28} ergs s^{-1} (0.1–1.8 keV); among solar-like stars, i.e., main-sequence stars of spectral type G, the RASS detection rate is $\approx 90\%$. The presence of many binary systems in the cluster is a key factor influencing the X-ray luminosity function. Short-period ($\sim$ a few days or less) binaries are anomalously X-ray bright, as might be expected; however, the X-ray luminosity functions of K and possibly M binaries of all types are significantly different from their single counterparts, confirming the results of Pye et al. for a smaller K star sample drawn from deep *ROSAT* pointings. Comparison with *Einstein Observatory* studies of a subset of Hyades stars demonstrates a general lack of significant (> a factor of 2) long-term X-ray variability. This may be the result of the dominance of a small-scale, turbulent dynamo in the younger Hyades stars compared to the large-scale, cyclic dynamo observed in the Sun.

Subject headings: binaries: close — open clusters and associations: individual (Hyades) — surveys — X-rays: stars

1. INTRODUCTION

The Hyades cluster is of unique importance to classical astronomy and to contemporary, space-based astronomical research. At a distance of only ~ 45 pc (Gunn et al. 1988; Schwan 1991), the Hyades is the nearest well-populated ($\gtrsim 450$ members) open star cluster in the Galaxy which is localized in the sky: the Ursa Major cluster is closer, but much sparser, with a nucleus of < 15 stars spread over 20° of sky (Soderblom & Mayor 1993). The Hyades is the prototype cluster for distance determination using the "moving-cluster" method and thus serves to define the zero-age main sequence which provides an absolute reference for the cosmic distance scale. Given its age of ~ 0.7 Gyr, nearly 8 times younger than the Sun, and its proximity, the Hyades cluster is of critical importance to studies of stellar evolution.

It is less generally appreciated that the Hyades cluster also occupies an important place in the study of the evolution of stellar activity on the main sequence. The pioneering work of Wilson (1966), Kraft (1967), and Skumanich (1972) established the fundamental connection among age, rotation, and chromospheric activity in solar-type cluster stars, with the Hyades playing a prominent role. Over the past 25 yr, greatly improved stellar rotational velocity measurements have become available for stars less massive than the Sun. At the same time, stellar optical spectroscopy using chromospheric diagnostics such as the Ca II and Hα lines has dramatically advanced with the advent of electronic detectors. Space-based observations of chromospheric, transition region, and coronal emission are now providing a wealth of diagnostic information on magnetic activity in main-sequence stars in both the solar neighborhood and in nearby open clusters. With this information, a picture has begun to emerge which suggests that, although the main sequence may represent the dullest period of a star's life in terms of *nuclear* evolution, a star's angular momentum, and consequently its stellar coronal and chromospheric activity, undergo dramatic changes during its residence on the main sequence (Stern 1984; Stauffer et al. 1991; Simon 1992).

Over a decade ago, Stern et al. (1981) reported the discovery of X-ray emission from roughly half the stars in the central 5° of the Hyades cluster. These results, obtained with the *Einstein Observatory*, demonstrated that the typical X-ray luminosity of a solar-type G star in the cluster was $\sim 10^{29}$ ergs s^{-1}, about 100 times that of a "mean" solar corona. Micela et al. (1988) continued the *Einstein* studies of the cluster, incorporating more observations outside the cluster center and deriving detailed X-ray luminosity functions for the main-sequence cluster members as a function of color (mass, spectral type). However, both these studies required many individual pointings (1° × 1°) in the Hyades region. Because of limitations in observing time, the *Einstein Observatory* studies could not even come close to covering all known or suspected cluster members: Stern et al.'s observational sample was limited to ≈ 85 Hyads with 48 detected, while the larger Micela et al. sample included ≈ 121 Hyads with 66 detected. Once these samples were further divided into subsamples of differing colors, not to mention single and binary stars, the sample statistics in each bin, while enough to determine gross differences among Hyades stars and the field or other clusters, were insufficient to provide unambiguous tests for many lines of inquiry.

Because there are now over 400 cluster members or candidates (see § 2), a more complete X-ray survey of the Hyades is clearly warranted. Fortunately, the means for such a study is now at hand in the form of the *ROSAT* All-Sky Survey (RASS; Voges 1992). Since the RASS constitutes a *complete* X-ray sky

[1] Also visitor at Max-Planck-Institut für Extraterrestrische Physik.

survey with a limiting sensitivity in the Hyades region comparable to that of a typical *Einstein* pointing (see § 6), we now have the opportunity to determine, in an unbiased fashion, the X-ray luminosity function for *all* known or possible members of the cluster established by proper motion, photometry, and radial velocity measurements, subject only to known limitations in X-ray sensitivity. In doing so, we hope to establish a true X-ray "baseline" study for all cluster members: given the uniqueness of the survey data and the lack of any similar proposed or planned all-sky X-ray survey, the RASS data may also prove to be the only complete X-ray study of the cluster for the next decade or more.

We have previously (Stern et al. 1992) provided a preliminary look at the RASS results for the Hyades (with appropriate cautionary remarks). In this paper, we discuss the completed analysis of the RASS data. The sky area covered comprises a $30° \times 30°$ region centered on the cluster and a number of smaller regions which incorporate outlying members or possible members. In total, our Hyades database includes over 1100 objects, containing both Hyades members and stars optically rejected as Hyades members. The membership list was compiled from the available literature with the aid of computerized files kindly provided to us by a number of Hyades researchers and also includes some unpublished data. The inclusion of rejected cluster candidates will, as we shall see, provide an interesting comparison between the detection rates for likely cluster members and a sample of field stars.

The plan of our paper is as follows: In § 2 we discuss the Hyades optical catalog. In § 3 we describe the RASS observations. In § 4 we discuss the methods of source detection and derivation of upper limits for undetected Hyads. In § 5 we examine the methods used to determine X-ray and optical positional coincidence and discuss the probabilities of correct source identification. In § 6 we provide X-ray fluxes and luminosities, as well as upper limits, and we discuss the detection rates and X-ray luminosity functions of main-sequence, giant, and white dwarf stars. In § 7 we discuss the dependence of our results on the presence of binary companions. In § 8 we provide comparisons of the RASS results with those of Stern et al. (1981) and Micela et al. (1988), and in § 9 we discuss our results in the context of stellar angular momentum evolution, as well as the theoretical implications of our comparison of long-term variability from the RASS and older *Einstein* imaging proportional counter (IPC) data.

2. OPTICAL CATALOG

Hyades membership may be determined via a combination of proper motions (e.g., van Bueren 1952; van Altena 1969; Hanson 1975; Pels Oort, & Pels-Kluyver 1975; Luyten, Hill, & Morris 1981; Schwan 1991; Reid 1992), photometry (Upgren 1974; Upgren & Weis 1977; Weis, Deluca, & Upgren 1979; Weis & Upgren 1982; Stauffer 1982; Weis 1983; Upgren, Weis, & Hanson 1985; Weis & Hanson 1988; Legget & Hawkins 1989; Reid 1993), and radial velocity (Wilson 1948; Kraft 1965; Stefanik & Latham 1985; Griffin et al. 1988). Probable members now total ≈ 450 or more (Reid 1993), although many of the fainter candidates ($V > 14$) have not been definitively confirmed by radial velocity measurements.

In compiling an optical catalog of the Hyades for comparison with our X-ray survey, we considered a number of factors. First, the initial catalog used for cross identifications between the X-ray and optical positions should include certain, probable, and even possible members of the cluster, since, as we shall see, X-ray emission is itself a statistical indicator of cluster membership. Second, membership "probabilities" given in the various proper motion surveys sometimes differ significantly, in some cases even for rather "well-known" members. For example, for the Hyades binary vB22 (HD 27130), Hanson's (1975) proper motion survey suggests a zero probability of membership, while the very same object (McClure 1982) has been used to estimate the distance to the cluster! Such discrepancies argue for relaxing the proper motion probability criterion for our initial optical catalog. Third, radial velocity measurements, which provide a definitive test of cluster membership (when combined with proper motion data and multicolor photometry), have generally been available only for stars with $V \lesssim 14$. Hence, for many of the stars in the newer proper motion surveys of, e.g., Reid (1992), confirmation of membership will require new radial velocity surveys at large telescopes.

For the purposes of our RASS optical input catalog, we compiled a list of objects which had been designated as Hyades candidates via the proper motion studies above and had been studied photometrically. E. Weis (private communication via J. Stauffer) kindly provided a computerized version of his Hyades membership cross-reference list (containing over 900 objects, including over 500 rejected Hyades candidates). This list formed the core of our optical catalog, with additional electronic files provided by H. Schwan and N. Reid (private communications). The initial list amounted to >1100 objects. We then noted candidates which had been photometrically rejected (Weis & Hanson 1988, and prior references cited therein) or rejected by Griffin et al. (1988) because of discordant radial velocities. Excluding new very faint ($V \gtrsim 17$) Hyads studied by Reid (1992, 1993), Leggett & Hawkins (1989), and Bryja et al. (1992), this left us with a list of 458 certain, probable, or possible members. Since some of these have low ($\lesssim 10\%$) proper motion candidacy probabilities, we will restrict our primary analyses to the higher probability candidates only, with the exception of roughly a dozen stars which, in spite of their low membership probabilities in the Hanson (1975) study, are both high-probability candidates in van Altena (1969) and have been classified as members by Griffin et al. (1988), Schwan (1991), or Reid (1993). The net effect of these adjustments leaves us with a final optical catalog of 440 Hyads. We decided to treat the faintest Hyades candidates from the Reid (1992) and Leggett & Hawkins (1989) studies separately, because the X-ray detection rate is extremely low for candidates in these surveys which had not been studied in earlier proper motion or photometry analyses (four detected out of 185 objects; see § 5.5). Although we do not include the optically rejected Hyades candidates (more than 500 in total) in our statistical analyses, we do provide a list of those detected in X-rays along with the low-probability Hanson (1975) proper motion candidates that are X-ray sources (§ 5.6).

Our RASS study area comprises over 900 deg^2, in contrast to even the largest proper motion surveys to date, which cover at most ~ 120 deg^2, primarily at the cluster center (Luyten et al. 1981; Reid 1993). Since, in our X-ray study, we have searched for X-ray sources *independently* of the optical catalog and used the optical catalog only to later verify identifications and perform X-ray upper limit analyses, we have potentially detected a number of Hyades members previously unidentified for lack of proper motion or photometric studies. However, determining *which*, if any, of the remaining X-ray sources are heretofore unrecognized cluster members will require a considerable additional effort in proper motion, photometric, and, if possible, radial velocity studies.

We note that the optical catalog described here differs significantly from that employed in our preliminary analysis of the RASS data (Stern et al. 1992). In that work, the entire Hyades region was *not* surveyed for all possible X-ray sources: instead, positions from a smaller optical input catalog were used to determine source likelihoods using the MPE Standard Analysis Software System (SASS; Voges 1992). Both these facts and the inclusion of 2 days of missing Position Sensitive Proportional Counter (PSPC) data (see Stern et al. 1992 and § 3) are likely to produce differences in the number of detected Hyads and estimated count rates.

3. OBSERVATIONS

The *ROSAT* Observatory carried out an all-sky X-ray survey between 1990 July 30 and 1991 January 25. Parts of the sky missed in this period were rescanned in 1991 February and 1991 August. During the all-sky survey observations, the *ROSAT* X-ray telescope (XRT) scanned the sky once per satellite orbit along great circles containing the north and south ecliptic poles, using the PSPC as the focal plane detector (Trümper 1983; Trümper et al. 1991; Pfeffermann et al. 1986). The scan period was synchronized to the orbital period of 96 minutes. In the 2° FWHM field of view of the PSPC, an X-ray source was visible for typically 20–30 per scan. An X-ray source in the Hyades cluster, which is near the ecliptic plane, was visible for about 2 days in the PSPC field of view. Total exposure times over the 2 day visibility interval amounted to 300–400 s. Due to its large angular extent (over 40° in R.A.), scanning of the Hyades cluster occupied more than 3 weeks during 1990 August. During this period, problems with a PSPC gas valve caused a data loss to occur when the very center of the Hyades cluster was scanned; the data for this region were obtained 6 months later on 1991 February 16–17. We note that the 1991 February data were actually taken with a different PSPC detector; however, we are not aware of any differences between the two PSPC detectors on board *ROSAT* that would affect the results of our analysis. In 1993 March, we therefore merged these data with the rest of the sky survey, allowing, for the first time, a complete analysis of the entire Hyades region. The 1991 February data typically have longer total exposure times (400–500 s) for a given region of sky than do the 1990 August data. Hence, the center of the Hyades cluster has a fainter limiting X-ray sensitivity than that quoted in the initial Stern et al. (1992) results (which were based only on the 1990 August data; see § 6).

4. ANALYSIS TECHNIQUES

We searched for sources in an $\approx 30 \times 30°$ region of the sky, centered at $\alpha = 4^h30^m$, $\delta = +15.0°$ (J2000), and close to the Hyades cluster center. As it turned out, 22 objects in our optical catalog lay outside this region, so we also searched for sources in $1° \times 1°$ regions centered at each of these 22 positions. All the source detection analysis was performed using the EXSAS software developed at MPE (Zimmermann et al. 1993). We conducted our analysis in two ways: (1) the entire $30° \times 30°$ region and outlying 22 smaller areas were searched for sources using the EXSAS LDETECT, MDETECT, and MAXLIK algorithms (see below), and (2) all objects in our optical catalog were then checked against the RASS data for detections or upper limits using the EXSAS algorithm COMPUTE/UPPER (see below). Because of the large number of photons ($\approx 1.2 \times 10^6$) contained in the principal $30° \times 30°$ area of our survey, for computational reasons we divided this region into nine overlapping subregions of $\approx 11° \times 11°$ each with a pixel size of $1'.6 \times 1'.6$. We compared the count rates and likelihoods for sources detected in those regions where two or more fields overlapped, and in all cases the differences were negligible. All source searches were conducted in three pulse-height (energy) bands: PSPC channels 11–181 (broad), 52–181 (hard), and 11–41 (soft). We note that the highest energy channel of the B and H bands is somewhat lower than that usually used by the standard *ROSAT* processing (SASS). We selected this after determining that the bulk of the Hyades detections contained very little, if any, flux in channels 181–240 ($\sim$1.8–2.4 keV). This is to be expected for sources with maximum temperatures $\lesssim$1–1.5 keV, as demonstrated in deep *ROSAT* pointed observations of the Hyades (Stern et al. 1994). Thus, the higher energy channels only contribute additional background and would therefore reduce the detection sensitivity of our survey.

The LDETECT, MDETECT, and MAXLIK techniques are described in Cruddace, Hasinger, & Schmitt (1988) and Zimmermann et al. (1993). Briefly, the LDETECT algorithm assumes nothing about the detector background and uses a sliding box (typically 3×3 pixels for the survey data) surrounded by a background region having a maximum extent of 5×5 pixels. A simple signal-to-noise (S/N) ratio is calculated for the inner box versus outer background region, and positions which meet a specific S/N threshold are flagged as possible source locations. Following this, a similar procedure is used, but now the background is taken from a separate smoothed "background map" generated by removing all the counts of the LDETECT sources. This is called the MDETECT procedure. Again, a list of possible sources which meet a simple S/N criterion is produced. Finally, for each of the possible source locations produced by the LDETECT and MDETECT algorithms, the maximum likelihood procedure (MAXLIK) described in detail in Cruddace et al. (1988) is performed, and sources which yield a likelihood statistic (ML) greater than a particular threshold are then accepted into a final source list. The MAXLIK procedure is used as the definitive source detection routine, because it computes a likelihood using the known instrumental point response function; hence, it will exclude LDETECT and MDETECT sources that are not consistent with pointlike objects or those that have an anomalous distribution of source counts versus position. In addition, it is the most sensitive, because it computes the overall likelihood photon by photon, allowing for the detection of weak, yet statistically significant, sources. For our second method of analysis, we used COMPUTE/UPPER, which is an identical algorithm to the MAXLIK algorithm, except that upper limits are calculated if the likelihood falls below a specified threshold. For COMPUTE/UPPER, we supplied a list of possible source locations, i.e., from our Hyades optical catalog.

Usually, the detection threshold for the *ROSAT* all-sky X-ray survey is chosen such that the probability of a false detection at a given position is 4.5×10^{-5} (ML $\approx$ 10). However, in the case of the Hyades, we lowered this threshold somewhat (to ML = 8, $P \approx 3.3 \times 10^{-4}$). This was done for two reasons: (1) to avoid missing possible sources near threshold, and (2) to allow for the fact that the number of independent positions in the sky (e.g., statistical trials) is considerably reduced because we are working from a preexisting optical catalog. Since our optical catalog contains $\sim 10^3$ possible source locations, a probability of 4.5×10^{-5} of any spurious

source detection is clearly too conservative: the adopted probability of 3.3×10^{-4} should result in <1 false Hyades detection for our entire study. Since this estimate depends somewhat upon the acceptable difference between optical and X-ray position, in § 5.3 we will examine the statistical distribution of such position differences in order to establish an appropriate criterion for a positive Hyades identification.

For sources which did not meet our X-ray detection criteria, we calculated upper limits in two ways:

1. Using the COMPUTE/UPPER algorithm, we first allowed the source position to be a free parameter, with the initial guess at the nominal position. This was done to allow for possible systematic errors in the optical positions and expected statistical errors in the X-ray positions. Our approach is conservative in the sense that it provides the highest upper limits for any possible X-ray source within a reasonable distance of a Hyades member. For our purposes, we chose 60″ as the largest reasonable difference between the upper limit position and the optical position. This limit was determined from the distribution of optical–X-ray positions for detected Hyades members (see § 5.3).

2. Again with COMPUTE/UPPER, we determined an upper limit to the count rate based upon fixing the X-ray position at the optical position. We adopted this upper limit only when COMPUTE/UPPER failed to produce an upper limit within the 60″ limit (i.e., the reported position at which the upper limit was calculated in method [1] was unreasonably far from the optical position). In all cases, we adopted a 95.4% level of confidence or "2 σ" upper limit to the PSPC count rate.

5. POSITIONS AND IDENTIFICATIONS

5.1. *An X-Ray Image of the Hyades Region*

For illustrative purposes, we have created a broadband (0.1–1.8 keV) composite image of the central 30° × 30° region studied, using all the photon event locations from the RASS data. We corrected for the varying exposure times ($\approx$300–600 s) across the region to derive count rates. Although one of the PSPC's great strengths is its ability to detect diffuse X-ray sky background features, for the purposes of this image we removed most of the diffuse features using a combination of the derived background map and a median filter technique. This was used to produce a "sourceless" image which could then be subtracted from the original image, resulting in a "source-enhanced" image shown in Figure 1 (Plate 24).

In this figure, individual sources are quite obvious. In the center of the image, a somewhat enhanced source density is attributable to the central Hyades objects (detected Hyads are indicated by circles). In the upper right can be seen another enhancement due to the Pleiades cluster (these data have been presented by Schmitt et al. 1993), and just to the left of the Pleiades two scans of the moon are visible. The Crab is partially visible at the extreme left of the upper portion of the image. Scattered throughout the image are other bright sources, many of which turn out to be active binary systems such as HR 1099 (V711 Tau). Although our procedure removes most of the nonuniformity in the residual background, there is still some evidence of "striping" in the image due to variations in solar-scattered radiation and other temporal changes in the PSPC background which are not due to diffuse sky features (see Freyberg 1994).

We emphasize that this X-ray image is used here for the purpose of illustration of our results and was *not* used as the basis for our source detection and count rate calculations, the details of which were discussed in § 4 above.

5.2. *Hyades Detections*

At the chosen detection threshold of our survey (ML = 8), there are >1900 X-ray sources (Hyads or other objects) in the 30° × 30° region shown in Figure 1. However, most of these sources are *not* Hyades members: even raising the likelihood threshold to ML = 10 reduces the number of detected sources by only 25%. Based upon previous experience with systematic and statistical errors in the RASS data, we initially settled upon a 60″ criterion for a positional match between an X-ray source and a Hyades optical candidate (§ 5.3). Of the ML $\geq$ 8 sources, only about 200 are associated with Hyades members or candidates in our 1100+ optical input catalog of Hyads or rejected Hyads, and 187 are associated with our 440 member final sample of Hyads.

In Figure 2 we plot the positions of the final Hyades sample and the X-ray detected stars (note that the Reid and Leggett-Hawkins stars, the many rejected Hyades candidates, and a few outlying Hyades members are not shown). In Figure 3 we plot the locations of the optical catalog stars on an H-R diagram and indicate which of those were detected in the Hyades survey. In Table 1 we provide a listing of probable and possible Hyades members in our survey for which we have measured PSPC count rates or upper limits. In column (1) of this table we provide the stellar identification (see table notes for details); column (2) contains the optical position (J2000, corrected for proper motion to epoch 1991.0), column (3) contains the difference in X-ray and optical positions in arcseconds, columns (4)–(7) contain the V and $B-V$ photometry with references (see table notes), columns (8)–(9) contain individually determined distances from either the Schwan (1991) or Hanson (1975) proper-motion surveys and the source indicated by an "H" or "S", column (10) contains a set of letter codes indicat-

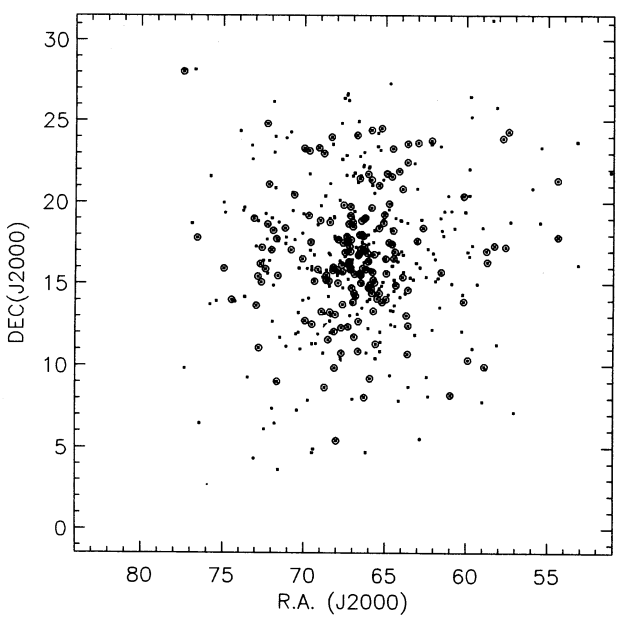

FIG. 2.—Sky positions of Hyades members in our optical catalog with RASS detections indicated by circles. Units of right ascension and declination are in decimal degrees.

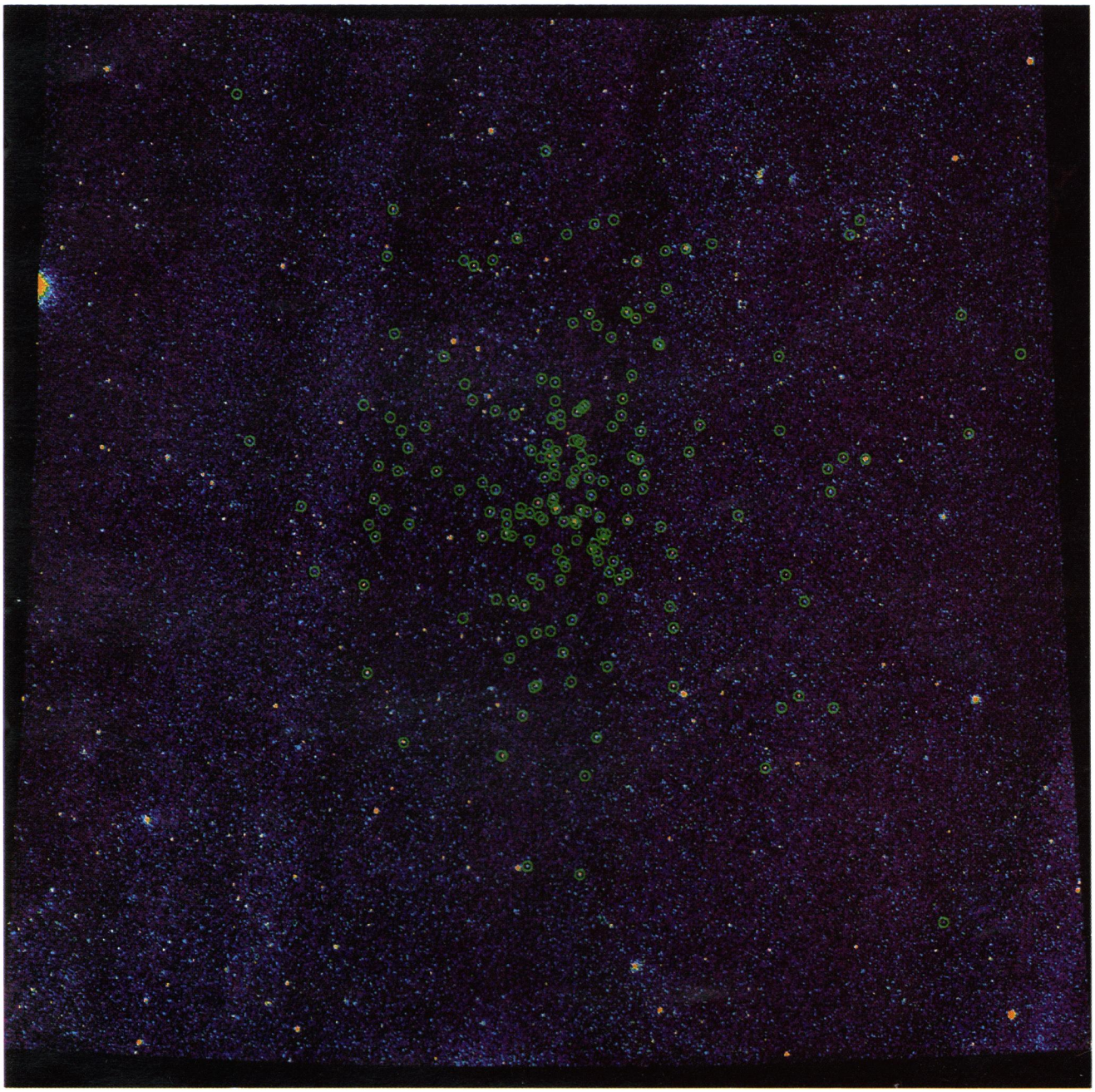

FIG. 1.—RASS X-ray image (broad band) of 30° × 30° region centered at 4^h30^m, +15° (J2000). Hyades members detected in X-rays are indicated by circles. North is up.

STERN, SCHMITT, & KAHABKA (see 448, 686)

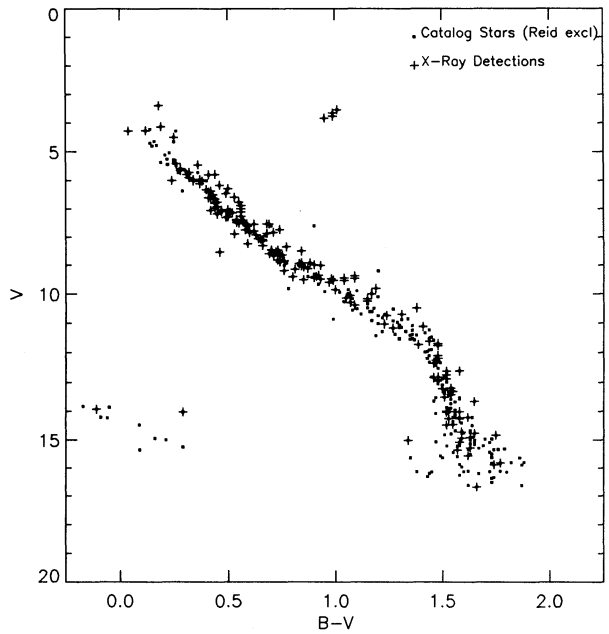

FIG. 3.—H-R diagram of the Hyades members in our optical catalog with RASS detections shown by crosses. Faint Hyads from the Reid (1992, 1993) and Leggett & Hawkins (1988) surveys have been excluded.

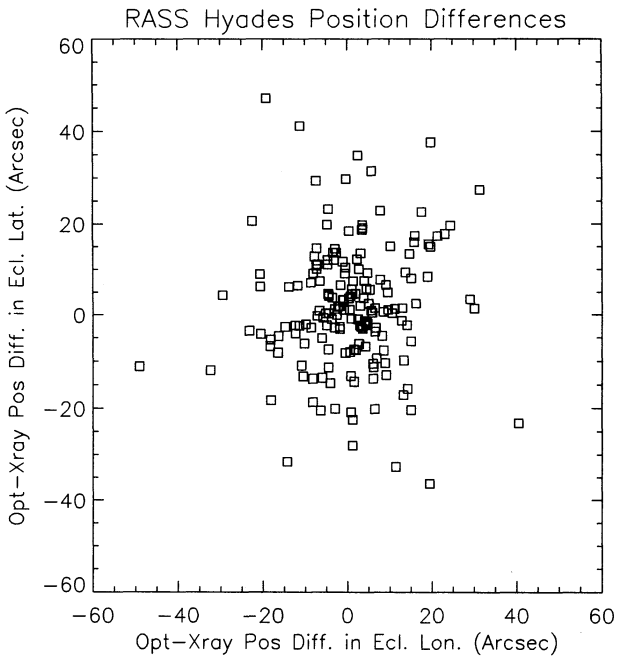

FIG. 4.—Difference in optical and X-ray positions in arcseconds plotted in ecliptic coordinates.

ing the type of binary system, if any (see table notes), column (11) contains the maximum likelihood ratio for X-ray source existence, and columns (12) and (13) contain the derived X-ray luminosity (in units of 10^{28} ergs s^{-1}), based upon (col. [12]) an assumed 45 pc distance and (col. [13]) using the distance, if available, from column (8).

5.3. *Distributions of X-Ray–Optical Positional Differences*

In order to assess the quality of the RASS positions as well as to determine the maximal position offset to be used for identification, we have studied the distribution between optical and X-ray positions for the Hyades members: in Figure 4 we show the difference (in arcseconds) between the optical and the X-ray position for all our Hyades detections, and in Figure 5 we plot a histogram of this distribution for ecliptic latitude, demonstrating that our data are well fit by a one-dimensional Gaussian distribution with $\sigma \approx 10''$; a similar histogram has been derived (but is not shown) for the distribution in ecliptic longitude. Combining these distributions, one expects the radial position offsets between X-ray and optical positions to be cumulatively distributed as $\Phi_1 = 1 - \exp[-(r^2/2\sigma^2)]$. On the other hand, for sufficiently small distances, spurious identifications will be (cumulatively) distributed as $\Phi_2 = B(2\pi r^2)$, with B denoting the number of "background" sources per unit area. One may then model the observed (cumulative) distribution of radial position offsets as a weighted sum of these two distributions, i.e.,

$$\Phi = A\left[1 - \exp\left(-\frac{r^2}{2\sigma^2}\right)\right] + (1 - A)B2\pi r^2 , \qquad (1)$$

where A, σ, and B are parameters to be determined (see Randich & Schmitt 1995). Since we know the total number of RASS sources ($\approx$60,000; Voges 1992), we expect that $B \approx 10^{-7}$ arcsec^2 and $\sigma \approx 15''$. In Figure 6 we plot the cumulative distribution of the X-ray sources identified with optically known Hyades members (*stepped curve*) and a model curve described by equation (1), with parameters values given by $A = 0.925$, $B = 1.1 \times 10^{-7}$ arcsec^2 and $\sigma = 14''$. As is obvious from Figure 6, the simple model given by equation (1) describes the observed distribution of positional differences quite well. There may be a discrepancy in the sense that for differences larger than 40″ the model curve is more or less flat while the observed differences still rise; however, the number of these cases is sufficiently small that this difference is statistically not significant. At any rate, if none of the 60,000 or so RASS sources were associated with our final 440 Hyades members,

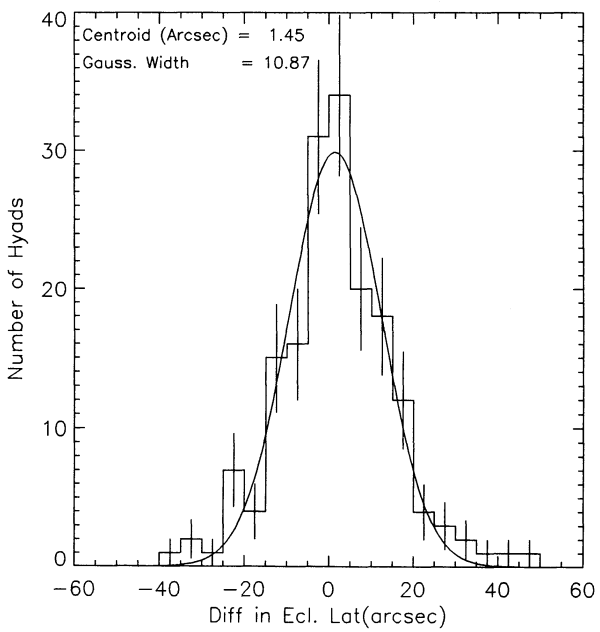

FIG. 5.—Histogram of difference between optical and X-ray positions in ecliptic latitude: 1 σ error bars are shown. Also plotted (*smooth curve*) is best-fit one-dimensional Gaussian distribution.

TABLE 1

HYADES SURVEY

Star[a]	α (J2000 Opt) h	m	s	δ °	′	″	Δ pos (″)	Photometry[b] V	ref	B-V	ref	Distance (pc)	ref	Binary[c] Codes	ML Ratio	X-Ray Luminosity[d] $L_X(45)$	$L_X(d)$
vB157	2	15	45.9	25	47	0.5	6.7	5.79	16	0.44	16				9.1	3.7 ± 1.7	
vB153	2	57	46.5	29	39	40.9	14.5	8.92	16	0.84	16				25.9	5.7 ± 1.4	
vB154	2	58	5.0	20	40	9.3	26.1	5.80	16	0.41	16	33.9	S		23.5	12.9 ± 3.5	7.3 ± 2.0
BD25:522	3	17	22.9	26	18	56.6	2.8	11.11	3	1.41	3			GV	108.1	20.7 ± 2.8	
vB1	3	17	26.4	7	39	20.9	12.7	7.40	16	0.57	16	43.1	S	A	17.3	3.7 ± 1.5	3.4 ± 1.3
vB2	3	17	32.8	7	41	24.5	13.0	7.78	16	0.62	16			GR ?	43.8	15.1 ± 3.0	
LP356-751	3	24	36.7	21	50	20.6		15.98	3						2.7	< 2.1	
LP413-78	3	32	34.4	16	9	17.5		14.21	3	1.64	3				5.5	< 2.9	
HD21847	3	32	39.9	35	39	33.4	33.7	7.30	17	0.49	17	52.5	S	MS	20.4	5.3 ± 1.6	7.2 ± 2.1
vB4	3	32	49.6	23	41	33.6		8.90	16	0.84	16	43.5	S		5.7	< 4.2	< 3.9
LP413-18	3	37	32.4	17	51	29.9	0.6	12.74	2	1.52	2				70.6	19.2 ± 3.1	
vB5	3	37	34.3	21	20	34.8	20.9	9.36	9	0.92	9	44.6	S		35.0	9.7 ± 2.2	9.5 ± 2.2
LP356-778	3	41	36.6	23	20	39.0		13.87	3	1.52	3				0.0	< 1.8	
LP413-89	3	41	55.6	18	45	38.2		13.34	3	1.53	3				1.8	< 1.8	
LP413-93	3	43	47.0	20	51	37.3		14.54	3						4.5	< 4.1	
GH7-15	3	48	12.0	7	8	46.3		10.85	11	1.34	11				1.4	< 2.5	
GH7-18	3	49	11.0	18	48	5.8		12.93	8	1.47	8				0.1	< 1.8	
LP357-4	3	49	42.3	24	19	3.5	5.2	14.21	8	1.62	8			S	46.5	11.2 ± 2.3	
V471TAURI	3	50	24.8	17	14	47.6	9.5	9.51	9	0.85	9			B	1936.2	229.6 ± 10.0	
vB170	3	51	1.9	23	54	10.6	20.8	10.25	9	1.15	9				10.2	3.0 ± 1.4	
GH7-26	3	52	34.2	11	15	41.9		13.73	9	1.54	9				0.0	< 1.1	
L7	3	52	41.3	25	48	16.4		11.15	14	1.30	14				0.0	< 1.9	
vB6	3	53	9.8	17	19	38.5	7.0	5.97	16	0.34	16	44.3	S		26.0	8.0 ± 2.2	7.7 ± 2.1
LP301-63	3	53	36.3	31	12	24.7		15.04	3						0.5	< 1.8	
GH7-33	3	54	52.6	16	18	56.9	16.2	14.25	9	1.58	9				56.4	15.7 ± 3.0	
vB7	3	55	6.5	16	59	55.4	5.8	8.99	9	0.90	9	43.4	S		15.1	2.3 ± 1.1	2.2 ± 1.0
GH7-41	3	55	21.8	9	47	19.6		14.47	3	0.09	3				0.0	< 1.4	
BD9:512	3	55	38.0	9	55	42.6	20.4	8.54	2	0.46	2				13.4	5.3 ± 1.9	
GH7-44	3	55	58.0	18	25	58.7		14.40	8	1.59	8				0.0	< 1.4	
GH7-43	3	56	2.8	7	47	29.2		15.76	4						0.1	< 1.3	
GH7-49	3	57	22.3	14	58	17.6		13.52	9	1.58	9				2.2	< 2.2	
AK8-111	3	58	34.2	11	2	37.5									3.9	< 2.3	
GH7-58	3	58	35.3	17	20	13.5		14.79	8	1.54	18				1.3	< 1.8	
LP357-279	3	58	54.1	25	13	11.2		14.03	3	1.56	3				1.2	< 1.3	
GH8-41	3	59	9.6	26	28	34.1		11.58	3	1.46	3				0.0	< 1.8	
LP414-479	3	59	13.6	20	25	41.2		13.57	3	1.58	3				0.0	< 1.9	
GH8-59	3	59	14.3	22	2	40.1		13.00	8	1.52	8				0.1	< 1.7	
LP414-25	3	59	15.2	16	39	52.4		15.83	6						0.0	< 1.4	
LP301-69	3	59	24.4	32	19	14.9	7.3	13.42	3	1.54	3				12.9	3.5 ± 1.4	
vB8	3	59	40.6	10	19	51.1	10.2	6.37	16	0.42	16	43.6	S		49.6	17.1 ± 3.1	16.0 ± 2.9
GH7-64	3	59	42.0	16	56	27.0		13.67	9	1.56	9				0.0	< 1.2	
LP414-30	4	0	15.5	19	24	36.7		16.13	6	1.72	18				3.2	< 2.8	
vB9	4	0	39.4	20	22	52.8	23.9	8.67	16	0.71	16			GR	10.5	5.5 ± 2.0	
GH7-71	4	0	44.9	13	54	23.1	10.4	14.84	11	1.75	11				20.0	6.5 ± 2.1	
LP474-749	4	0	59.5	14	20	45.3		15.21	3	1.52	18				2.0	< 2.1	
GH7-73	4	1	11.1	12	5	53.7		11.48	11	1.45	11				0.0	< 1.9	
GH7-80	4	2	53.0	18	24	26.5		15.30	4	1.67	18				0.1	< 2.6	
BD19:650	4	3	39.0	19	27	17.5		10.17	9	1.08	9				0.0	< 2.2	
GH7-85	4	3	41.6	14	59	29.7		14.95	5	0.16	5				1.3	< 1.1	
vB160	4	3	56.4	8	11	47.4	5.6	5.46	16	0.36	16				91.4	22.9 ± 3.4	
LP414-50	4	4	27.1	20	24	30.0		15.89	3	1.87	18				1.4	< 2.7	
GH7-88	4	5	25.6	19	26	31.9		11.41	14	1.35	14				0.0	< 2.0	
BD17:679	4	5	39.6	17	56	15.6		9.32	9	0.90	9				3.7	< 4.2	
GH7-89	4	6	2.2	18	15	3.3		12.83	11	1.51	11				0.0	< 2.2	
vB10	4	6	16.1	15	41	53.1	27.6	7.85	16	0.60	16	48.4	S		15.8	5.8 ± 2.1	6.7 ± 2.4
LP357-160	4	6	20.4	23	25	24.9		14.14	6	1.56	6				4.0	< 3.6	
LP414-1100	4	6	20.6	19	1	38.8		16.13	2	1.60	18				2.5	< 2.0	
GH7-92	4	6	34.6	13	32	56.9		13.52	9	1.47	9				7.0	< 5.1	
BD14:653	4	7	1.1	15	20	4.9		10.49	14	1.18	14				1.9	< 2.1	
vB11	4	7	42.0	15	9	46.1		6.01	16	0.40	16	41.8	S	GV T A	6.6	< 6.6	< 5.7
BD16:558	4	7	43.2	16	31	7.1		9.94	9	1.02	9				0.5	< 2.0	

TABLE 1—*Continued*

Star[a]	α (J2000 Opt) h	m	s	δ °	′	″	Δ pos (″)	Photometry[b] V	ref	B-V	ref	Distance (pc)	ref	Binary[c] Codes	ML Ratio	X-Ray Luminosity[d] $L_X(45)$	$L_X(d)$
GH7-104	4	8	11.1	16	52	23.1		11.52	11	1.44	11				1.6	< 1.6	
GH7-105	4	8	26.6	12	11	30.7		11.28	9	1.33	9				0.0	< 1.2	
BD23:622	4	8	35.9	23	46	4.2	21.4	9.44	14	0.90	14				8.8	2.0 ± 1.0	
GH8-53	4	8	39.7	23	33	27.9		12.86	11	1.52	11			GV	0.9	< 1.8	
BD7:604	4	9	24.4	8	7	50.4		10.86	8	0.99	8				0.0	< 1.1	
GH7-112	4	9	28.9	17	7	54.0		15.35	15	0.09	15				0.1	< 0.9	
BD8:642	4	9	49.7	9	18	12.6		10.10	11	1.20	11				0.0	< 2.3	
VA9	4	9	57.4	15	25	3.3		16.12	6	1.77	19				4.1	< 2.9	
vB13	4	10	42.4	18	25	23.9	4.1	6.62	16	0.42	16	47.2	S		24.6	7.4 ± 2.2	8.1 ± 2.4
LP301-82	4	10	43.3	32	56	7.5		12.10	2	1.44	2				0.0	< 1.3	
GH7-120	4	11	6.0	18	55	44.6		15.63	6	1.73	18				3.1	< 2.3	
vB14	4	11	19.9	5	31	25.0		5.73	16	0.36	16	38.3	S	GR	5.4	< 4.5	< 3.3
GH7-122	4	11	27.4	15	59	33.2		15.15	9	1.65	9	47.5	H		1.9	< 3.4	< 3.8
BD23:635	4	11	55.9	23	38	9.2	11.6	9.38	14	1.09	14			GR GP B UW	594.9	84.3 ± 5.7	
LP414-1570	4	12	3.4	20	49	51.7		16.52	3	1.73	18				2.7	< 1.8	
VA43	4	12	7.4	17	37	34.8	10.0	14.77	9	1.65	9	45.9	H		17.7	6.2 ± 2.0	6.4 ± 2.1
VA45	4	12	21.5	16	15	4.9		13.99	11	1.53	11	36.1	H		6.2	< 8.2	< 5.2
HZ 2, EG 3	4	12	44.5	11	52	1.1		13.86	15	-0.05	15				1.6	< 1.3	
LP357-309	4	12	47.5	22	23	30.0		15.73	3						1.2	< 2.2	
VA50	4	13	5.4	15	14	53.1		15.81	6	1.82	19	47.1	H		5.4	< 3.4	< 3.7
VA54	4	13	52.1	15	21	55.1		15.01	10	1.65	10	50.4	H		0.1	< 2.2	< 2.8
GH7-130	4	14	17.1	8	42	1.4									0.0	< 1.8	
vB17	4	14	25.7	14	37	30.4	51.6	8.46	16	0.70	16	47.3	S		25.4	11.6 ± 2.8	12.9 ± 3.1
vB18	4	14	27.3	12	26	7.3	15.4	8.06	16	0.64	16	48.5	S		45.7	15.4 ± 3.2	17.8 ± 3.7
GH7-132	4	14	29.8	18	43	48.0		14.49	8	1.64	8				6.2	< 4.5	
vB16	4	14	30.4	22	27	7.0	12.1	7.05	16	0.42	16	60.0	S		59.4	13.5 ± 2.4	24.0 ± 4.3
vB15	4	14	32.3	23	34	29.7	21.8	8.09	16	0.66	16	44.9	S		54.3	12.9 ± 2.4	12.8 ± 2.4
vB19	4	14	34.3	10	42	4.5	6.3	7.12	16	0.51	16	47.0	S		59.9	17.9 ± 3.4	19.5 ± 3.7
VA68	4	14	51.8	13	3	18.4	2.4	10.74	1	1.24	1	42.5	H	C	12.9	6.4 ± 2.2	5.7 ± 2.0
VA72	4	15	10.2	14	23	55.3		11.57	1	1.37	1	50.6	H		0.0	< 1.5	< 1.9
VA75	4	15	33.5	15	42	23.7		10.97	11	1.29	11	45.8	H		0.3	< 1.4	< 1.4
VA76	4	15	34.6	16	45	45.7		15.20	9	1.58	10	54.6	H		0.0	< 1.1	< 1.6
vB162	4	15	42.4	20	49	11.2	20.5	7.83	16	0.71	16	49.1	S	GR B T	56.3	13.5 ± 2.5	16.1 ± 2.9
vB20	4	15	46.0	15	24	2.5	27.9	6.32	16	0.40	16	48.7	S		24.6	8.0 ± 2.2	9.3 ± 2.6
VA83	4	16	1.2	16	58	59.6		15.14	9	1.63	18	49.1	H		5.1	< 3.1	< 3.7
GH7-141	4	16	3.5	18	51	32.7		14.07	9	1.52	9				0.0	< 1.2	
GH7-142	4	16	13.1	18	53	3.9		11.90	9	1.45	9				0.8	< 1.1	
VA88	4	16	25.2	14	10	18.1		15.33	9	1.62	10	40.2	H		5.2	< 4.0	< 3.2
vB21	4	16	33.1	21	54	26.8	23.3	9.14	9	0.81	9	50.3	S		17.1	6.0 ± 1.8	7.5 ± 2.2
GH7-145	4	16	40.3	7	50	46.1		13.58	8	1.54	8				1.5	< 1.3	
VA94	4	16	43.1	16	49	21.0		15.85	6	1.77	18	58.0	H		0.0	< 1.2	< 2.0
VA96	4	16	54.2	16	21	25.7		14.35	3	1.55	3	49.4	H		0.0	< 1.5	< 1.8
BD18:614	4	17	25.1	19	1	47.3		10.83	9	1.22	9				1.1	< 1.7	
VA106	4	17	28.0	14	54	4.9	13.0	14.46	10	1.55	10	47.7	H		16.5	3.7 ± 1.4	4.2 ± 1.5
vB22	4	17	38.9	16	56	52.2	15.0	8.35	16	0.77	16	50.8	S	GR GP B C	172.3	34.3 ± 3.8	43.8 ± 4.8
VA112	4	17	39.6	12	24	53.9		15.32	9	1.79	9	41.0	H		0.7	< 2.6	< 2.2
VA115	4	17	47.5	13	39	42.9		12.65	1	1.52	1	46.9	H		0.0	< 1.0	< 1.1
VA118	4	17	51.4	15	13	39.1		15.59	6	1.57	19	48.1	H		2.1	< 3.0	< 3.5
VA119	4	17	54.8	16	32	40.8	13.1	14.01	9	1.53	9	43.3	H		19.6	7.3 ± 2.1	6.8 ± 1.9
VA122	4	17	55.4	14	32	47.1		15.00	9	1.63	9	54.2	H		0.0	< 1.9	< 2.8
vB23	4	18	1.8	18	15	24.5	20.4	7.53	16	0.69	16	49.3	S	B T C GR	60.1	15.2 ± 2.7	18.3 ± 3.2
VA129	4	18	8.4	13	19	53.1		14.68	11	1.63	11	41.5	H		6.5	< 4.7	< 4.0
VA127	4	18	8.7	17	24	59.9		16.15	6	1.80	18	59.4	H		1.4	< 3.4	< 6.0
BD22:669	4	18	9.9	23	17	20.8	32.0	9.48	9	0.98	9			GR	376.7	72.9 ± 5.8	
VA131	4	18	12.7	16	5	53.3		16.20	6	1.67	19	51.4	H		1.1	< 1.8	< 2.3
vB25	4	18	19.1	16	5	18.4		9.60	1	0.98	1	45.5	S		2.5	< 2.7	< 2.7
VA135	4	18	21.8	17	25	18.9	13.9	10.00	1	1.17	1	44.5	H	GP	124.8	25.2 ± 3.3	24.7 ± 3.3
vB24	4	18	22.8	21	34	43.9	26.3	5.65	16	0.28	16	57.4	S	B T MD	33.9	9.0 ± 2.2	14.6 ± 3.5
LP414-158	4	18	34.0	18	21	55.6		16.09	3						2.6	< 1.7	
VA141	4	18	42.1	12	30	38.5		15.51	6	1.63	10	42.8	H		2.7	< 1.9	< 1.7
VA146	4	18	46.9	13	21	59.2		11.98	1	1.42	1	43.8	H		6.4	< 5.1	< 4.8
LP358-676	4	18	55.1	27	17	41.6		15.00	5	0.21	5				0.0	< 0.6	

TABLE 1—*Continued*

Star[a]	α (J2000 Opt) h	m	s	δ °	′	″	Δ pos (″)	Photometry[b] V	ref	B-V	ref	Distance (pc)	ref	Binary[c] Codes	ML Ratio	X-Ray Luminosity[d] $L_X(45)$	$L_X(d)$
LP474-266	4	18	56.0	9	23	43.0		16.26	6						0.0	< 1.8	
vB26	4	18	58.0	19	54	23.9	51.1	8.62	16	0.74	16	48.2	S		12.2	3.6 ± 1.3	4.2 ± 1.5
GH7-163	4	19	3.4	19	32	41.5		15.28	9						0.0	< 0.8	
vB27	4	19	8.0	17	31	29.2	4.8	8.46	1	0.73	1	50.0	S		32.9	8.8 ± 2.0	10.9 ± 2.5
VA162	4	19	20.0	14	18	59.8		12.82	1	1.45	1	44.0	H		0.0	< 0.9	< 0.9
L44	4	19	30.0	21	45	15.6	0.7	14.03	13	1.52	13				51.1	18.5 ± 3.1	
vB28	4	19	47.9	15	37	38.7	6.0	3.65	16	0.99	16	46.8	S		423.5	61.0 ± 4.8	65.9 ± 5.2
vB29	4	19	54.8	16	31	21.0	15.1	6.89	16	0.56	16	47.3	S	GP GV T C	87.5	18.8 ± 2.8	20.8 ± 3.1
vB30	4	19	57.5	14	2	6.6	12.5	5.59	16	0.28	16	45.8	S		62.1	13.5 ± 2.4	14.0 ± 2.5
vB31	4	20	13.0	19	14	0.4	5.0	7.46	16	0.57	16	46.4	S		45.9	11.6 ± 2.2	12.3 ± 2.4
vB32	4	20	25.1	18	44	33.8	15.5	6.11	16	0.37	16	47.1	S		59.6	13.7 ± 2.4	15.1 ± 2.6
LP415-543	4	20	27.5	18	53	50.2		15.34	6	1.76	18				2.7	< 1.7	
LP414-167	4	20	29.6	21	22	41.7		15.50	6	1.73	6				4.6	< 4.1	
vB33	4	20	36.3	15	5	41.7		5.26	16	0.22	16	49.3	S		0.0	< 1.1	< 1.3
vB34	4	20	52.5	13	51	51.8	7.7	6.17	16	0.46	16	50.3	S	B T C GR	94.2	19.9 ± 2.9	24.8 ± 3.6
VA203	4	20	55.8	14	51	34.9		16.62	8	1.62	10	49.5	H		4.9	< 3.1	< 3.8
LP358-716	4	21	0.6	24	31	9.4	17.4	14.85	3						11.4	1.7 ± 0.8	
GH7-173	4	21	16.2	11	25	39.6		14.49	9						4.3	< 4.2	
LP358-717	4	21	16.9	23	11	50.4		16.86	3						2.9	< 2.4	
VA208	4	21	19.7	12	2	38.4		16.34	9	1.74	10	42.8	H	S	2.3	< 3.1	< 2.8
LP475-381	4	21	23.4	10	52	2.0		15.63	3	1.35	18				3.9	< 2.8	
vB35	4	21	31.7	21	2	23.4	8.2	6.80	16	0.44	16	51.0	S		40.3	9.2 ± 2.0	11.8 ± 2.5
vB36	4	21	32.3	18	25	3.5	14.1	6.81	16	0.44	16	49.0	S		23.5	6.1 ± 1.7	7.2 ± 2.0
vB37	4	21	34.8	14	24	35.3	12.1	6.61	16	0.41	16	49.3	S		79.5	15.0 ± 2.5	17.9 ± 3.0
VA216	4	21	34.9	14	41	43.0		15.64	6	1.50	18	56.6	H		0.0	< 1.5	< 2.4
VA213	4	21	35.3	16	53	40.1		15.44	6	1.72	18	47.3	H		6.9	< 3.4	< 3.8
LP358-134	4	21	53.3	24	14	23.9		15.13	4						5.7	< 3.5	
LP358-534	4	21	56.2	23	25	5.8		13.44	6	1.53	6				7.6	< 3.5	
vB38	4	22	3.3	14	4	38.3	13.8	5.72	16	0.32	16	47.6	S	B T	11.2	4.4 ± 1.5	5.0 ± 1.7
BD10:568	4	22	25.6	11	18	20.2	35.6	9.81	9	1.19	9	44.3	S	GR GP UW	13.6	3.3 ± 1.2	3.2 ± 1.2
GH7-180	4	22	30.0	10	26	4.6		12.66	11	1.52	11				0.0	< 0.9	
VA242	4	22	39.2	18	16	10.1		13.00	10	1.52	10	60.3	H		2.4	< 2.4	< 4.4
LP415-30	4	22	42.9	20	34	11.8		14.90	4	1.64	9				5.2	< 2.7	
vB40	4	22	44.2	15	3	22.5	6.3	7.00	16	0.56	16	41.9	S	B T C A GR	178.6	26.9 ± 3.1	23.4 ± 2.7
vB39	4	22	44.6	16	47	28.5	12.4	7.87	16	0.68	16	38.2	S	GR	55.3	14.1 ± 2.4	10.1 ± 1.8
vB41	4	22	56.2	17	32	32.1	16.7	3.76	16	0.99	16	49.4	S	GR MP	8.7	3.0 ± 1.2	3.6 ± 1.5
GH7-183	4	22	59.8	13	18	58.7	20.2	13.65	11	1.65	11	48.9	H		11.8	3.6 ± 1.4	4.2 ± 1.6
VA260	4	23	1.3	15	13	41.9	3.8	16.68	6	1.66	10	49.3	H		8.9	2.3 ± 1.1	2.8 ± 1.3
LP415-688	4	23	11.4	21	3	31.0		15.33	6						1.7	< 1.6	
VA262	4	23	12.3	15	42	47.4	4.5	15.82	9	1.77	10	43.2	H		15.6	4.3 ± 1.5	4.0 ± 1.4
vB42	4	23	22.3	21	22	44.5	40.5	8.85	16	0.76	16	52.0	S	GP	8.5	2.6 ± 1.1	3.5 ± 1.5
vB43	4	23	22.7	19	39	29.9	13.9	9.40	9	0.91	9	52.6	S	GR	8.9	2.3 ± 1.0	3.1 ± 1.4
VA275	4	23	23.6	14	25	41.1	8.0	14.94	9	1.59	9	48.5	H		13.4	3.6 ± 1.3	4.1 ± 1.5
vB45	4	23	24.8	16	46	39.5		5.64	16	0.30	16	49.9	S	B	5.7	< 4.7	< 5.8
vB173	4	23	25.1	15	45	47.4		10.52	1	1.27	1	42.2	S		1.7	< 3.6	< 3.2
vB44	4	23	30.4	24	24	19.2	20.9	7.18	16	0.45	16	56.1	S		49.5	9.6 ± 1.8	14.8 ± 2.8
vB46	4	23	32.4	14	40	13.5	17.9	9.12	1	0.87	1	45.1	S		16.3	4.4 ± 1.5	4.5 ± 1.5
VA282	4	23	42.8	15	52	51.8		14.76	9	1.59	10	46.4	H		3.5	< 2.8	< 2.9
VA288	4	23	50.2	14	55	18.0	9.2	13.30	10	1.55	10	39.3	H	S	53.9	11.0 ± 2.1	8.4 ± 1.6
GH7-192	4	23	50.9	9	12	17.6	11.5	12.88	9	1.52	9			GR	99.1	20.4 ± 3.0	
VA294	4	23	54.3	14	3	8.3		10.88	1	1.31	1	44.9	H		3.7	< 2.6	< 2.6
VA292	4	23	55.5	16	21	15.6		14.23	10	-0.06	10	45.0	H		0.0	< 1.4	< 1.4
LP358-722	4	23	56.8	22	10	51.9		15.18	3						4.6	< 2.4	
VA297	4	23	58.9	16	43	17.8		12.53	1	1.48	1	57.1	H		0.0	< 1.0	< 1.6
vB47	4	24	6.1	17	26	39.3		4.80	16	0.15	16	48.2	S		0.4	< 1.9	< 2.2
L38	4	24	7.7	22	7	9.1		11.02	14	1.20	14				4.6	< 2.1	
vB50	4	24	12.5	14	45	29.7	3.1	7.61	1	0.59	1	45.9	S	GP? C MP	386.0	53.0 ± 4.3	55.1 ± 4.5
vB49	4	24	12.8	16	22	43.9	19.7	8.24	16	0.59	16	52.7	S		27.3	7.0 ± 1.8	9.6 ± 2.5
vB48	4	24	14.6	21	44	10.3	1.6	7.14	16	0.52	16	44.0	S		156.3	20.1 ± 2.4	19.2 ± 2.3
VA314	4	24	15.4	12	14	50.9		16.13	3	1.38	18				5.4	< 2.6	
vB174	4	24	16.7	18	0	11.4		9.99	1	1.06	1	52.0	H		3.5	< 2.4	< 3.2
vB51	4	24	22.3	17	4	44.1	11.9	6.97	16	0.44	16	51.9	S		9.0	3.6 ± 1.4	4.8 ± 1.8

TABLE 1—*Continued*

Star[a]	α (J2000 Opt) h	m	s	δ °	′	″	Δ pos (″)	Photometry[b] V	ref	B-V	ref	Distance (pc)	ref	Binary[c] Codes	ML Ratio	X-Ray Luminosity[d] $L_X(45)$	$L_X(d)$
VA321	4	24	28.1	15	53	3.8		14.98	9	1.70	18	51.0	H		0.0	< 1.2	< 1.6
vB52	4	24	28.3	16	53	10.1	11.8	7.80	16	0.60	16	43.9	S	GP?	42.6	10.8 ± 2.1	10.2 ± 2.0
VA326	4	24	31.3	13	55	43.2		16.63	6	1.87	10	49.5	H		0.0	< 2.2	< 2.7
VA329	4	24	38.2	15	54	34.9		15.35	8	1.74	18	54.4	H		0.0	< 1.0	< 1.5
vB140	4	24	43.2	4	41	59.7		8.93	16	0.77	16	51.2	S	B GR?	0.0	< 1.6	< 2.0
GH7-199	4	24	44.0	10	46	19.1		14.02	6	1.53	9				1.7	< 1.7	
VA334	4	24	47.8	15	52	30.0	14.0	11.61	1	1.44	1	53.5	H	GR C	75.3	13.5 ± 2.2	19.0 ± 3.2
vB53	4	24	57.1	19	2	29.9	2.9	5.97	16	0.37	16	49.0	S	T	47.0	9.1 ± 1.8	10.8 ± 2.1
vB175	4	25	0.1	16	59	6.9		10.27	1	1.04	1	59.5	H		0.3	< 1.5	< 2.6
VA351	4	25	13.4	17	16	6.5	10.6	13.19	10	1.54	10	47.9	H	UW SP	147.1	24.2 ± 2.8	27.4 ± 3.2
GH7-204	4	25	14.5	18	58	24.9	14.7	12.82	12	1.48	12				20.9	5.0 ± 1.4	
VA352	4	25	16.4	16	18	9.8		16.37	4	1.73	18	46.1	H		0.7	< 0.7	< 0.7
GH7-206	4	25	16.6	8	4	0.0	42.2	12.61	8	1.58	8				21.0	6.1 ± 1.8	
LP358-724	4	25	18.0	23	3	40.4		13.96	3	1.56	3				4.1	< 2.5	
GH7-207	4	25	18.7	8	4	47.9		14.92	9						3.0	< 4.1	
vB54	4	25	22.0	22	17	40.0		4.22	16	0.14	16	50.0	S		0.0	< 0.8	< 1.0
vB55	4	25	24.9	22	11	57.7		5.28	16	0.25	16	47.1	S		0.0	< 0.7	< 0.7
VA354	4	25	25.1	17	54	58.2	0.5	11.17	1	1.27	1				16.3	5.2 ± 1.5	
vB56	4	25	29.8	17	55	39.6	30.6	4.28	16	0.04	16	46.6	S		27.1	6.7 ± 1.6	7.2 ± 1.7
vB57	4	25	37.1	15	56	28.1	4.7	6.46	16	0.49	16	51.2	S	GR T C A	235.5	30.7 ± 3.1	39.8 ± 4.0
LP415-829	4	25	41.8	19	0	47.3		14.82	13	1.51	18				0.0	< 1.1	
VA362	4	25	46.9	17	32	41.1		15.84	9	1.73	10	41.9	H		2.5	< 1.7	< 1.5
vB176	4	25	47.3	18	1	3.8	1.6	9.01	1	0.93	1	61.9	H	GR T C	22.9	6.3 ± 1.6	11.8 ± 3.0
VA368	4	25	50.3	15	0	9.7		16.25	9	1.58	10	48.7	H		0.0	< 1.2	< 1.4
VA371	4	25	51.5	13	30	9.5		15.21	9	1.69	10	40.3	H		0.9	< 0.7	< 0.5
vB58	4	25	51.7	18	51	50.7	11.0	7.53	16	0.68	16	46.1	S	GV GP T A	121.1	19.7 ± 2.5	20.7 ± 2.6
VA382	4	26	4.1	17	7	15.2	16.6	15.56	6	1.62	18	50.1	H		20.8	4.7 ± 1.3	5.8 ± 1.6
LP358-242	4	26	4.2	21	37	55.4		13.02	6	1.48	6				0.2	< 1.1	
VA383	4	26	4.5	15	2	28.7	8.5	12.18	1	1.48	1	49.9	H		8.7	1.4 ± 0.7	1.7 ± 0.9
vB59	4	26	5.8	15	31	27.4	4.2	7.49	16	0.54	16	47.9	S	GR	118.1	21.8 ± 2.8	24.7 ± 3.1
vB62	4	26	18.5	21	28	13.7	7.4	7.38	16	0.54	16	51.0	S	B GR	28.0	5.1 ± 1.3	6.5 ± 1.7
vB60	4	26	18.7	22	48	48.0		4.28	16	0.26	16	48.3	S	T	0.0	< 1.1	< 1.3
vB141	4	26	20.8	15	37	6.1	9.6	4.50	16	0.25	16	46.0	S	T	1411.6	132.4 ± 6.1	138.4 ± 6.4
LP415-875	4	26	21.6	18	0	0.8	17.9	15.89	4	1.74	18				8.1	2.2 ± 1.0	
vB63	4	26	24.6	16	51	11.9	32.2	8.08	1	0.65	1	46.6	S	GR GP C	66.5	12.4 ± 2.1	13.3 ± 2.2
vB64	4	26	40.1	16	44	48.7	12.3	8.14	1	0.66	1	46.6	S		42.2	8.0 ± 1.7	8.6 ± 1.8
VA404	4	26	42.7	12	41	11.7	4.4	10.48	1	1.38	1	39.2	H	GV GP UW	16.2	5.1 ± 1.6	3.8 ± 1.2
LP358-250	4	26	47.4	24	56	58.3		16.40	6						0.0	< 1.0	
L58	4	26	47.8	21	14	4.5		11.24	14	1.36	14				5.4	< 3.7	
BD10:576	4	26	48.1	10	52	15.2	14.0	9.45	9	1.04	9	49.0	S	MP	8.1	2.5 ± 1.2	3.0 ± 1.4
VA407	4	26	54.2	13	8	17.1		10.48	1	1.15	1	44.4	H		0.9	< 1.4	< 1.4
LP358-268	4	27	3.4	24	6	15.3	7.0	16.04	6						9.3	2.6 ± 1.1	
VA420	4	27	16.4	17	14	32.1		13.05	1	1.48	1	47.1	H		0.0	< 0.7	< 0.7
VA432	4	27	23.9	14	7	7.3		15.87	9	1.58	10	48.1	H		1.2	< 0.7	< 0.8
vB177	4	27	25.2	14	15	38.9	43.4	10.39	1	1.09	1	44.7	H	GR	10.5	2.3 ± 1.0	2.3 ± 1.0
GH8-60	4	27	35.5	21	48	19.3		14.69	11	1.59	11				0.0	< 1.1	
vB65	4	27	35.9	15	35	20.9	12.7	7.42	16	0.54	16	46.5	S		67.6	10.7 ± 1.9	11.4 ± 2.0
LP415-108	4	27	36.4	19	26	44.7		15.64	6	1.86	18				5.5	< 3.5	
vB66	4	27	46.1	11	44	11.0	4.3	7.51	16	0.55	16	48.4	S		93.3	17.1 ± 2.5	19.8 ± 2.8
vB179	4	27	46.9	14	25	4.1	21.1	9.49	1	0.93	1	46.8	H		9.5	2.7 ± 1.0	2.9 ± 1.1
BD18:638	4	27	56.7	19	3	38.4		11.29	11	1.22	11	62.0	S		0.0	< 1.2	< 2.3
BD18:639	4	27	58.9	18	30	1.0	13.9	10.14	9	1.05	9			B GR	12.0	3.4 ± 1.2	
GH7-224:	4	27	59.1	18	45	32.7	7.3	14.22	12	1.58	12			GR UW	9.5	2.6 ± 1.0	
vB67	4	28	0.3	21	37	11.4		5.72	16	0.27	16	51.6	S		2.1	< 2.0	< 2.6
vB178	4	28	4.4	13	52	4.9	29.2	9.03	1	0.84	1	52.7	S	GP C	22.1	6.3 ± 1.6	8.6 ± 2.2
LP535-80	4	28	7.6	7	56	42.6		15.09	3						2.6	< 2.4	
vB189	4	28	10.7	16	28	15.8		11.08	1	1.36	1	44.2	H		2.0	< 1.4	< 1.4
H430	4	28	22.3	13	49	21.6		16.31	6	1.43	10	41.7	H		1.8	< 1.8	< 1.5
vB68	4	28	23.4	14	44	27.4	19.2	5.90	16	0.32	16	48.3	S		15.5	3.9 ± 1.2	4.5 ± 1.4
VA486	4	28	28.6	17	41	45.9	13.5	12.10	1	1.48	1	49.0	H	UW GR	189.4	27.4 ± 2.9	32.4 ± 3.4
vB71	4	28	34.6	15	57	45.5	18.9	3.83	16	0.95	16	47.8	S	GR	1398.3	113.6 ± 5.5	128.5 ± 6.2
vB69	4	28	37.2	19	44	26.7	30.6	8.64	16	0.75	16	51.5	S	B GR	15.1	5.8 ± 1.7	7.6 ± 2.2

TABLE 1—*Continued*

Star[a]	α (J2000 Opt) h	m	s	δ °	′	″	Δ pos (″)	Photometry[b] V	ref	B-V	ref	Distance (pc)	ref	Binary[c] Codes	ML Ratio	X-Ray Luminosity[d] $L_X(45)$	$L_X(d)$
vB70	4	28	37.4	19	10	51.0	21.9	3.54	16	1.01	16	47.3	S		9.1	2.2 ± 1.0	2.4 ± 1.1
VA490	4	28	39.2	16	58	12.8	9.2	13.92	10	-0.11	10	47.3	H		22.0	4.2 ± 1.2	4.7 ± 1.4
vB72	4	28	39.5	15	52	15.4	34.2	3.39	16	0.18	16	47.3	S	B	15.1	3.8 ± 1.3	4.2 ± 1.4
vB73	4	28	48.3	17	17	7.6	20.3	7.82	1	0.60	1	45.4	S		53.5	11.2 ± 2.0	11.4 ± 2.1
vB74	4	28	50.2	13	2	51.0		5.03	16	0.23	16	48.5	S		0.6	< 0.7	< 0.9
vB190	4	28	50.7	16	17	21.1	16.1	10.70	1	1.31	1	49.8	H	GR GP UW C	148.4	21.0 ± 2.5	25.6 ± 3.1
VA502	4	28	52.3	15	58	54.2		11.97	1	1.43	1	46.3	H		8.0	< 5.2	< 5.5
vB75	4	28	59.7	16	9	32.7	13.1	6.59	16	0.53	16	52.0	S	GR T A	56.6	11.2 ± 2.0	14.9 ± 2.6
VA512	4	29	0.0	16	20	47.4	23.6	14.26	9	1.53	10	49.9	H		19.4	5.4 ± 1.4	6.6 ± 1.7
GH7-237	4	29	0.9	18	40	25.2	5.2	13.21	3	1.50	3				14.3	4.7 ± 1.5	
LP358-730	4	29	11.3	26	14	48.5		12.93	3	1.49	3				0.0	< 1.4	
VA529	4	29	12.2	15	16	25.5		12.34	1	1.49	1	45.3	H		0.0	< 1.4	< 1.4
VA537	4	29	16.1	12	21	37.4	11.2	14.72	9	1.59	10	45.7	H		8.1	1.3 ± 0.6	1.3 ± 0.6
vB77	4	29	20.5	17	32	41.5	4.2	7.03	16	0.50	16	47.2	S	B GR	125.9	21.8 ± 2.7	24.0 ± 3.0
vB78	4	29	30.3	17	51	47.2	53.4	6.92	16	0.45	16	47.3	S		10.1	5.5 ± 1.7	6.1 ± 1.9
vB181	4	29	30.8	16	14	42.0		10.34	1	1.15	1	49.4	H		0.7	< 2.0	< 2.4
vB76	4	29	30.9	26	40	17.1	18.9	9.19	3	0.76	3	56.4	S		8.1	2.6 ± 1.2	4.0 ± 1.9
vB79	4	29	31.4	17	53	35.9	24.2	8.94	1	0.83	1	47.1	S		10.9	3.9 ± 1.4	4.3 ± 1.5
LP358-731	4	29	36.7	26	34	22.8		16.09	3						5.9	< 4.1	
L73	4	29	37.4	21	40	5.1		14.21	13	1.55	13				0.0	< 1.4	
LP358-348	4	29	38.9	22	52	58.9		11.52	7	1.30	7				1.3	< 1.3	
VA559	4	29	55.5	16	54	51.1	17.4	12.84	1	1.46	1	48.2	H		27.8	6.8 ± 1.7	7.8 ± 1.9
vB180	4	29	57.7	16	40	22.4		9.05	1	0.85	1	49.3	S		5.6	< 4.0	< 4.8
LP358-352	4	30	16.5	26	22	26.1		16.50	3						1.1	< 1.3	
vB81	4	30	18.0	19	50	26.0	35.3	7.10	16	0.47	16	52.7	S	GR	86.5	17.7 ± 2.8	24.3 ± 3.8
VA575	4	30	23.8	17	30	0.0	10.3	14.48	9	1.52	9	52.3	H		8.2	1.8 ± 0.9	2.4 ± 1.2
GH7-246	4	30	33.9	14	44	53.5		14.68	9	1.56	9				0.0	< 1.7	
vB82	4	30	33.9	16	11	37.8		4.78	16	0.17	16	48.1	S		0.8	< 1.2	< 1.4
vB182	4	30	34.9	15	44	2.3	8.0	9.01	1	0.84	1	53.3	S	B GR GP C	25.9	5.1 ± 1.4	7.2 ± 1.9
vB84	4	30	37.1	13	43	25.7	4.5	5.41	16	0.26	16	45.5	S		55.7	9.3 ± 1.8	9.5 ± 1.8
vB83	4	30	38.7	15	41	30.9		5.48	16	0.26	16	48.6	S		0.6	< 0.9	< 1.0
LP358-733	4	30	44.7	22	37	48.5		14.79	3						0.0	< 1.6	
vB85	4	30	46.8	16	8	55.3	30.2	6.51	16	0.43	16	48.7	S	C	201.1	32.1 ± 3.3	37.6 ± 3.9
LP358-371	4	30	55.5	24	50	17.6		16.21	6						2.0	< 1.8	
vB86	4	30	57.1	10	45	6.2	7.3	7.04	16	0.47	16	54.4	S		77.8	11.2 ± 1.9	16.4 ± 2.8
VA607	4	30	57.3	12	18	13.7	7.2	14.01	9	1.58	9	40.2	H		55.4	9.3 ± 1.8	7.4 ± 1.4
VA610	4	31	10.9	16	23	46.0		15.14	9	1.58	10	44.7	H		1.2	< 2.5	< 2.4
vB87	4	31	15.7	20	7	59.5		8.60	16	0.74	16	50.4	S		6.6	< 6.3	< 7.9
VA622	4	31	28.9	17	43	7.8		11.91	1	1.44	1	47.8	H		5.8	< 5.2	< 5.9
VA627	4	31	37.0	17	42	36.7	19.6	9.53	1	0.99	1	44.7	H	B GR GP C	24.0	9.4 ± 2.2	9.3 ± 2.1
VA637	4	31	43.5	15	2	27.9	14.6	12.25	1	1.47	1				9.2	4.3 ± 1.6	
VA638	4	31	44.6	15	37	46.6		12.19	1	1.43	1	59.5	H	GV	0.0	< 1.3	< 2.2
vB89	4	31	51.6	15	51	6.1	28.3	6.02	16	0.34	16	47.6	S		19.3	5.1 ± 1.6	5.7 ± 1.7
vB191	4	31	52.4	15	29	58.6		11.07	1	1.30	1	41.5	H		0.0	< 1.5	< 1.3
vB90	4	32	4.8	5	24	36.2	7.5	6.40	16	0.41	16	43.3	S		36.0	9.1 ± 1.9	8.4 ± 1.7
VA657	4	32	7.8	17	39	53.0		15.23	9	1.57	10	53.2	H		0.0	< 1.2	< 1.6
VA673	4	32	23.6	17	45	3.0	17.1	14.02	3	0.29	3	44.5	H		9.0	2.7 ± 1.3	2.7 ± 1.2
VA677	4	32	25.6	13	6	47.4	3.8	11.03	1	1.23	1	43.6	H	GR C	232.8	33.4 ± 3.3	31.3 ± 3.1
VA674	4	32	28.9	17	54	17.2		15.45	6	1.55	19	59.9	H		3.9	< 3.4	< 6.0
LP415-183	4	32	37.8	19	2	47.9		15.10	6	1.72	18				2.8	< 2.9	
LP475-1095	4	32	37.8	9	51	6.1	3.8	11.69	2	1.48	2				128.8	17.5 ± 2.4	
BD18:647	4	32	40.8	19	6	48.4		10.51	3	1.10	3				5.7	< 2.9	
VA683	4	32	45.3	12	3	59.7	45.6	15.02	9	1.34	18	50.4	H		10.7	3.6 ± 1.3	4.5 ± 1.6
vB91	4	32	50.1	16	0	20.7	30.9	8.92	1	0.88	1	53.1	S	GR T C MD	16.5	3.5 ± 1.3	4.9 ± 1.8
vB92	4	32	59.4	15	49	8.2	27.2	8.66	9	0.74	9	53.6	S		11.3	4.7 ± 1.7	6.7 ± 2.4
LP358-735	4	33	5.0	23	33	20.9		16.59	3						1.7	< 0.9	
L74	4	33	23.5	23	59	25.6	6.3	12.62	12	1.52	12			GV GP UW	191.1	31.1 ± 3.4	
VA709	4	33	26.9	13	2	43.7		13.22	10	1.52	10	43.0	H		4.0	< 3.0	< 2.7
VA714	4	33	35.4	11	59	34.3		15.57	8	1.49	18	59.3	H		0.0	< 0.7	< 1.2
BD20:774	4	33	37.0	21	9	0.9		10.70	9	1.23	9				1.9	< 1.6	
vB93	4	33	37.9	16	45	44.8		9.43	6	0.89	6	59.4	S		6.4	< 4.2	< 7.4
L65	4	33	41.8	19	0	50.4		10.75	9	1.20	9				0.0	< 1.5	

TABLE 1—*Continued*

Star[a]	α (J2000 Opt) h	m	s	δ °	′	″	Δ pos (″)	Photometry[b] V	ref	B-V	ref	Distance (pc)	ref	Binary[c] Codes	ML Ratio	X-Ray Luminosity[d] $L_X(45)$	$L_X(d)$
LP415-2120	4	33	42.7	18	45	59.2	24.0	15.28	6	1.63	18				10.0	3.3 ± 1.3	
VA722	4	33	44.9	12	42	40.8		14.21	3	-0.09	3	46.1	H		0.0	< 0.9	< 1.0
vB94	4	33	46.6	13	15	7.0	7.3	6.62	16	0.43	16	51.9	S		89.0	17.6 ± 2.7	23.4 ± 3.6
vB95	4	33	50.4	14	50	42.4		4.65	16	0.25	16	47.3	S	B T	0.0	< 1.5	< 1.7
VA726	4	33	56.6	16	52	10.7	42.6	15.08	8	1.58	18				14.1	3.3 ± 1.3	
vB96	4	33	58.4	15	9	48.8	16.4	8.50	1	0.84	1	50.1	S	GR T C	27.1	8.7 ± 2.1	10.8 ± 2.6
VA731	4	34	5.3	14	13	3.0		12.33	11	1.44	11	47.8	H		5.1	< 3.4	< 3.9
L79	4	34	11.0	11	33	28.6	34.8	11.73	9	1.39	9				16.0	6.0 ± 1.7	
vB183	4	34	32.2	15	49	39.1		9.67	1	0.92	1	61.6	S		1.4	< 3.8	< 7.2
vB97	4	34	35.3	15	30	16.5	14.0	7.92	1	0.63	1	51.4	S		16.3	7.7 ± 2.1	10.1 ± 2.8
VA750	4	34	39.9	15	12	32.4	9.6	12.35	1	1.46	1				62.4	16.2 ± 2.9	
L77	4	34	50.1	20	23	39.8		11.14	9	1.31	9			GR	5.4	< 3.6	
AK2-188	4	35	2.5	8	39	32.5	5.5	11.76	7	1.48	7				79.8	14.4 ± 2.3	
VA760	4	35	5.5	13	10	25.2		15.07	9	1.47	18	51.3	H		4.6	< 4.2	< 5.4
LP358-739	4	35	13.3	22	59	18.2	18.3	16.01	3						10.4	3.4 ± 1.4	
LP475-176	4	35	24.6	10	44	52.6		15.96	3	1.59	18				2.2	< 1.9	
VA763	4	35	28.3	15	23	57.9		16.11	9	1.62	10	54.6	H		0.0	< 0.9	< 1.3
VA776	4	35	48.5	13	17	16.9	10.1	14.91	11	1.63	11	42.8	H		9.4	4.4 ± 1.6	4.0 ± 1.5
LP415-1574	4	35	52.0	19	47	44.5		15.21	6	1.57	18				1.8	< 1.5	
L86	4	36	4.1	18	53	18.9	19.4	13.51	13	1.51	13				37.4	10.0 ± 2.2	
vB99	4	36	5.2	15	41	2.0		9.40	6	0.87	6	56.0	S		6.0	< 4.8	< 7.5
vB100	4	36	29.1	23	20	27.2	23.6	6.02	16	0.38	16	46.3	S		12.5	6.1 ± 1.8	6.5 ± 1.9
L87	4	36	38.9	18	36	56.7		13.26	12	1.51	12				1.3	< 1.2	
vB101	4	36	40.7	15	52	9.2	7.5	6.65	16	0.44	16	53.9	S		146.8	25.9 ± 3.3	37.1 ± 4.7
HD286900	4	36	41.3	11	55	0.6		9.20	17	1.20	17	31.4	S		0.0	< 1.2	< 0.6
LP475-1419	4	37	14.5	11	19	27.0		16.14	3	1.45	18				3.1	< 2.5	
vB102	4	37	31.9	15	8	45.2	15.8	7.54	16	0.62	16	44.7	S	GR MD	72.2	15.8 ± 2.7	15.5 ± 2.7
LP415-266	4	37	32.1	16	45	32.0	45.0	15.36	4	1.57	18				9.2	4.0 ± 1.6	
LP535-101	4	37	44.3	4	54	10.0		14.73	3						2.1	< 1.8	
L118	4	37	58.1	4	40	9.1		11.52	9	1.36	9				4.2	< 3.4	
vB103	4	38	8.9	16	2	0.8	15.6	5.79	16	0.31	16	52.1	S		8.1	2.7 ± 1.2	3.6 ± 1.6
LP475-214	4	38	9.4	11	19	5.6		16.19	3	1.44	18				2.1	< 1.5	
vB104	4	38	9.8	12	30	37.3	9.4	4.27	16	0.12	16	46.1	S		8.4	3.4 ± 1.5	3.6 ± 1.6
LP415-1692	4	38	10.5	15	49	17.9		15.80	6	1.88	18				3.3	< 1.8	
L83	4	38	24.9	17	32	33.2	17.9	10.17	8	1.15	8			B GR GP UW	10.0	3.5 ± 1.4	
LP415-1718	4	38	31.5	17	2	26.8		14.97	6	1.73	18				4.2	< 3.2	
LP358-479	4	38	42.9	21	44	16.0		16.70	6						0.0	< 1.3	
vB105	4	38	50.8	23	9	2.7	7.8	7.53	16	0.58	16	44.9	S		61.0	14.2 ± 2.4	14.1 ± 2.4
LP415-292	4	38	54.7	19	10	55.7	0.6	14.00	6	1.52	6				72.7	14.2 ± 2.4	
vB106	4	38	57.3	14	6	20.0		7.96	16	0.67	16	48.6	S	GR	3.1	< 3.0	< 3.5
vB107	4	39	6.6	7	52	15.8		5.39	16	0.25	16	49.8	S		0.0	< 1.5	< 1.8
vB108	4	39	16.8	15	55	2.6		4.70	16	0.14	16	57.2	S	T	2.9	< 2.3	< 3.7
BD12:623	4	39	50.9	12	43	42.6	4.9	10.06	9	1.07	9	47.0	S		10.1	3.0 ± 1.3	3.3 ± 1.4
L85	4	39	56.7	23	8	16.8		11.41	3	1.38	3				0.0	< 1.0	
vB109	4	40	5.9	23	18	16.9	15.8	9.41	3	0.80	3	71.1	S		11.8	3.7 ± 1.4	9.2 ± 3.4
GH8-68	4	40	12.6	19	17	9.6		13.64	8	1.46	8				1.7	< 2.0	
LP475-242	4	40	23.8	13	58	45.1		15.25	18	0.29	18				0.0	< 0.9	
vB185	4	40	25.4	16	30	49.2	2.2	9.47	9	1.09	9	51.6	S	B GR GP UW	8.9	2.9 ± 1.3	3.8 ± 1.6
LP415-1816	4	40	28.2	18	5	16.7		15.05	6	1.65	18				4.6	< 3.2	
LP475-251	4	41	1.6	10	59	40.2		13.83	3	-0.17	3				0.0	< 1.0	
LP415-333	4	41	16.4	15	57	8.0		14.75	6	1.60	18				1.7	< 1.0	
LP475-1699	4	41	28.4	12	0	35.7		12.88	3	1.50	3				2.0	< 1.6	
L81	4	41	29.8	13	13	17.5		11.23	8	1.44	8			GR UW	0.0	< 1.6	
LP535-109	4	41	47.0	7	16	29.1		15.85	2						3.7	< 2.8	
LP475-1747	4	42	4.3	11	55	15.3		13.37	3	1.51	3				2.2	< 1.5	
LP415-348	4	42	19.1	17	41	37.5		15.02	6						2.3	< 1.6	
LP415-345	4	42	30.4	20	27	12.5	3.5	13.28	4	1.54	4				50.1	10.9 ± 2.2	
LP415-353	4	42	51.3	19	29	11.1		14.97	6						2.2	< 1.1	
LP415-3051	4	42	58.6	20	36	16.5		15.06	6						6.0	< 2.7	
BD16:646	4	43	15.3	17	4	9.7	13.6	9.86	9	1.00	9			B GR	41.4	9.1 ± 2.0	
LP359-243	4	43	24.4	24	17	50.4		14.07	3	1.47	3				2.1	< 1.3	
vB111	4	44	25.4	11	8	47.6		5.40	16	0.25	16	46.5	S		2.1	< 1.9	< 2.1

TABLE 1—*Continued*

Star[a]	α (J2000 Opt) h	m	s	δ °	′	″	Δ pos (″)	Photometry[b] V	ref	B-V	ref	Distance (pc)	ref	Binary[c] Codes	ML Ratio	X-Ray Luminosity[d] $L_X(45)$	$L_X(d)$
LP415-2132	4	44	28.3	17	51	10.6		15.80	4						1.4	< 2.9	
LP359-245	4	44	32.0	23	56	27.8		15.61	3						0.0	< 2.0	
LP415-406	4	44	34.8	17	27	4.2		15.96	4						0.0	< 0.9	
LP415-2037	4	44	44.0	18	24	27.5	15.0	15.19	4						24.8	6.8 ± 1.8	
vB112	4	46	2.0	11	42	17.3		5.37	16	0.19	16	66.0	S		0.0	< 0.9	< 1.9
LP416-26	4	46	15.5	18	46	27.1		15.76	6						6.0	< 3.6	
L119	4	46	19.0	3	38	10.9		10.93	9	1.27	9				1.0	< 1.5	
LP416-471	4	46	27.1	17	37	32.4		16.10	3						0.0	< 1.7	
vB142	4	46	30.4	15	28	19.1	16.1	8.30	9	0.66	9	50.3	S	GR	9.3	3.8 ± 1.4	4.7 ± 1.8
vB113	4	46	45.6	9	1	2.8	3.9	7.26	16	0.56	16	41.2	S	GR	116.5	24.0 ± 3.3	20.1 ± 2.8
BD17:782	4	46	49.4	17	44	53.8	7.9	9.60	9	0.97	9	49.1	S	GR	25.2	7.0 ± 1.8	8.3 ± 2.1
BD20:820	4	47	9.2	20	52	59.1		9.85	11	1.06	11				0.0	< 1.5	
LP359-42	4	47	10.2	24	1	10.8		12.28	3	1.48	3				1.1	< 0.7	
AK2-1315	4	47	18.2	6	27	12.4		11.33	7	1.42	7				3.3	< 2.7	
L93	4	47	25.9	23	3	3.8		10.69	6	1.12	6				4.7	< 3.0	
L91	4	47	34.9	14	53	22.0		11.54	9	1.35	9				0.0	< 1.0	
vB114	4	47	37.6	18	15	31.3	30.6	8.53	16	0.72	16	49.0	S	GR	11.6	2.9 ± 1.2	3.4 ± 1.4
BD25:733	4	47	41.1	26	9	2.5		10.61	9	1.17	9				1.5	< 0.8	
LP476-631	4	47	50.3	12	41	27.3		15.88	3						5.0	< 3.8	
LP536-60	4	47	54.2	7	22	15.8		16.67	3						1.7	< 1.8	
LP416-565	4	47	56.9	19	1	26.0		13.09	3	1.50	3				2.0	< 2.0	
L95	4	48	1.5	17	3	19.9	5.9	11.12	3	1.41	3			GR GP	28.5	7.7 ± 1.9	
LP416-570	4	48	31.7	16	23	17.9		12.42	3	1.47	3				0.0	< 1.1	
vB115	4	48	41.4	21	6	4.8	22.1	9.06	9	0.85	9	50.5	S	GR	14.8	3.9 ± 1.3	4.9 ± 1.7
LP416-56	4	48	59.7	15	36	16.0		15.72	6						1.6	< 1.7	
vB116	4	49	3.5	18	38	28.3	14.7	8.99	9	0.84	9	46.5	S		16.1	3.7 ± 1.3	4.0 ± 1.4
LP416-572	4	49	11.3	17	42	57.0		14.00	3	1.52	3				1.1	< 0.8	
vB117	4	49	12.3	24	48	14.2	14.7	9.53	3	1.04	3	48.2	S	B GR	155.0	27.2 ± 3.2	31.2 ± 3.7
LP416-573	4	49	28.2	19	16	37.6		16.63	3						0.3	< 1.6	
vB118	4	49	32.1	15	53	19.3	5.9	7.74	16	0.58	16	50.2	S		18.2	5.3 ± 1.6	6.6 ± 2.0
LP536-63	4	49	51.8	6	6	31.8		14.73	3	1.63	3				0.0	< 1.4	
BD16:655	4	50	0.7	16	24	41.7		10.61	14	1.16	14				0.0	< 1.6	
vB119	4	50	23.9	17	12	9.4	5.1	7.11	16	0.56	16	44.3	S	GR	96.5	16.3 ± 2.5	15.8 ± 2.4
vB120	4	50	33.8	15	5	0.5	3.5	7.73	16	0.74	16	52.7	S	GR GP	38.5	8.8 ± 1.9	12.1 ± 2.7
vB121	4	50	48.5	16	12	37.3	12.7	7.29	16	0.50	16	52.1	S	B GR	53.8	11.2 ± 2.2	15.0 ± 2.9
vB122	4	51	12.5	11	4	4.7	10.5	6.77	16	0.55	16	52.0	S	GV A	181.7	31.6 ± 3.6	42.2 ± 4.8
vB123	4	51	22.7	18	50	24.0		5.11	16	0.21	16	53.1	S		1.1	< 1.3	< 1.7
vB143	4	51	23.2	15	26	0.4	24.0	7.89	16	0.53	16	67.4	S		29.5	7.5 ± 1.8	16.7 ± 4.2
LP416-94	4	51	48.8	17	16	22.0		11.38	3	1.28	3				2.5	< 1.8	
vB124	4	51	49.9	13	39	18.3	9.0	6.29	16	0.50	16	54.2	S	B GR	90.2	17.8 ± 2.7	25.8 ± 3.8
HD31003	4	52	23.8	4	20	1.6		8.50	20		20				0.0	< 1.1	
BD18:746	4	52	24.0	18	59	49.4	24.0	10.29	14	1.07	14				14.0	4.7 ± 1.6	
LP359-94	4	52	47.6	22	38	53.4		11.54	9	1.30	9				2.6	< 1.8	
BD23:755	4	53	0.7	23	29	16.4		10.56	11	1.08	11				0.0	< 1.2	
LP536-70	4	53	56.4	9	16	2.3		15.96	3						7.6	< 5.5	
LP476-645	4	54	37.2	14	11	16.7		16.14	3						0.0	< 1.4	
LP416-130	4	54	43.9	19	40	51.5		13.89	8	1.54	8				6.0	< 3.6	
vB126	4	54	58.4	19	29	7.4		6.37	16	0.29	16	59.8	S		2.8	< 2.7	< 4.7
LP359-262	4	55	49.0	24	21	46.5		15.01	3						0.6	< 1.9	
BD13:741	4	57	0.9	13	54	42.6		10.92	9	1.17	9				5.0	< 3.2	
LP476-648	4	57	28.0	13	56	40.7		16.48	3						0.3	< 0.8	
vB127	4	57	49.5	14	0	7.9	18.8	8.89	16	0.74	16	61.9	S		8.8	3.3 ± 1.3	6.2 ± 2.5
LP416-589	4	59	27.6	19	20	37.6		15.70	3						3.1	< 2.2	
vB128	4	59	44.3	15	55	0.9	20.5	6.76	16	0.45	16	46.1	S		29.1	7.5 ± 1.9	7.9 ± 2.0
BD19:832	4	59	49.4	19	58	0.0		9.82	7	0.78	7				0.0	< 1.4	
L104	5	1	36.0	13	55	59.2		11.39	9	1.36	9				0.0	< 1.0	
vB129	5	3	5.5	21	35	22.5		4.64	16	0.16	16	57.2	S		0.0	< 1.1	< 1.8
vB187	5	3	7.6	13	43	50.5		9.00	9	0.76	9	61.2	S		6.1	< 4.4	< 8.2
vB151	5	5	40.4	6	27	54.5		9.92	9	0.95	9	54.4	S	GR?	0.2	< 1.1	< 1.6
BD17:841	5	6	18.0	17	48	59.4	11.8	8.82	7	0.73	7	63.3	S		19.2	5.3 ± 1.6	10.5 ± 3.2
HD240676	5	6	58.4	28	9	19.2		9.90	17	1.10	17	48.1	S		1.1	< 0.8	< 1.0
AK7-858	5	7	36.0	18	41	33.0		11.43	8	1.19	8				0.0	< 1.0	

TABLE 1—*Continued*

Star[a]	α (J2000 Opt) h	m	s	δ °	′	″	Δ pos (″)	Photometry[b] V	ref	B-V	ref	Distance (pc)	ref	Binary[c] Codes	ML Ratio	X-Ray Luminosity[d] $L_X(45)$	$L_X(d)$
vB130	5	9	20.1	9	49	45.2		5.41	16	0.26	16	55.5	S	B	0.0	< 0.8	< 1.3
vB132	5	9	45.5	28	2	0.2	10.7	8.59	17	0.69	17	72.0	S	GV A	18.8	4.1 ± 1.3	10.4 ± 3.4
vB131	5	9	45.5	28	1	47.6	0.5	6.00	16	0.24	16	60.1	S		14.9	3.9 ± 1.3	7.0 ± 2.4
vB168	5	37	4.3	17	2	25.3		5.44	16	0.22	16				0.0	< 0.9	
HD38835	5	49	25.2	18	37	5.3		7.60	17	0.70	17				0.0	< 1.1	
HD39681	5	54	36.7	11	29	7.7		7.60	17	0.90	17				0.0	< 1.3	
vB169	6	2	23.4	9	38	47.5	15.0	4.13	16	0.19	16				59.5	12.7 ± 2.3	

[a] For members with multiple designations, the name used is determined by the following order of preference: vB (van Bueren 1952), VA (van Altena 1969), BD (Bonner Durchmusterung), GH 7 or GH 8 (Giclas, Burnham, & Thomas 1962), L (Pels et al. 1975), LP (Luyten et al. 1981), H (Hanson 1975), OS (Osvald 1954), AK (Artyukhina & Khopolov 1975, 1976), HD, or other designation. A table of cross-referenced Hyades members provided by E. Weis was used in selecting the primary designation.

[b] Optical photometry references are as follows: (1)–(3) Weis & Hanson 1988; (4)–(6) Upgren et al. 1985; (7) Weis 1983; (8)–(9) Weis & Upgren 1982; (10) Stauffer 1982; (11) Weis et al. 1979; (12)–(13) Weis 1992, unpublished photometry; (14) Pels et al. 1975; (15) Eggen 1969; (16) Morel & Mangnenat 1978; (17) Schwan 1991; (18) Reid 1992; (19) Hanson 1975; (20) Griffin et al. 1988.

[c] Binary notations: GR = spectroscopic binary as noted in Griffin et al. 1988; GP = photometric binary as noted in Griffin et al. 1988; GV = visual binary as noted in Griffin et al. 1988, B = spectroscopic binary listed in Batten et al. 1989; C = photometric binary from Carney 1982; T = photometric binary as noted by Bettis 1975; S = photometric binary as noted by Stauffer 1982; UW = photometric binary as noted by Upgren & Weis 1977; A = visual binary in ADS catalog; MD = definite speckle binary in Mason et al. 1993; MP = probable speckle binary in Mason et al. 1993; MS = suspected speckle binary in Mason et al. 1993; SP = spectroscopic binary or triple based on unpublished data (Stauffer, private communication).

[d] Units are 10^{28} ergs s^{-1}.

we would expect ≈0.6 incorrect identifications just by chance. This fact together with the curves shown in Figure 6 shows that spurious identifications will not affect our Hyades X-ray catalog in any noticeable fashion.

In summary, we emphasize that our RASS Hyades observations are not significantly affected by spurious sources (i.e., by mistaking a count fluctuation as a true X-ray source) or by incorrect identifications (i.e., by incorrectly identifying a real X-ray source with a Hyades member).

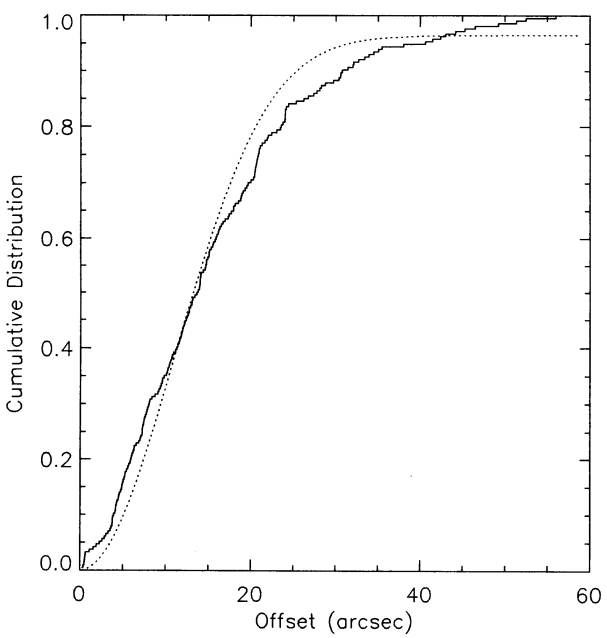

FIG. 6.—Cumulative distribution of X-ray–optical position differences (*histogram*). Smooth dotted line is fitted model based upon two-dimensional Gaussian.

5.4. *White Dwarf and Giant Detections*

In the completed RASS Hyades study, we have detected the single white dwarf EG 37 = VA 490 and EG 38 = VA 673 = HZ 9, a red dwarf/white dwarf binary (see, e.g., Stauffer 1982). The detection of EG 37 has been discussed in Stern et al. (1992), and although the count rate reported here is slightly different than in the preliminary survey, the count rate uncertainty is smaller in the completed survey (0.029 ± 0.009 vs. 0.045 ± 0.016 in the preliminary survey), and the results are within 1 σ of each other. The smaller uncertainty in the completed survey is due primarily to increased exposure time.

In the preliminary survey, EG 38/HZ 9 was *not* detected at our limit of ≈0.02 counts s^{-1}. However, in the completed survey, this source is seen at 0.019 ± 0.009 counts^{-1}, consistent with our earlier nondetection and the increased exposure of the completed survey. As Pye et al. (1994) point out, however, the X-rays in HZ 9 are most likely coming from the red dwarf in the system, not from the photosphere of the relatively cool (15,600 K) white dwarf EG 38.

The completed RASS observations of the Hyades region have also confirmed the detections of all four Hyades giants as X-ray emitters. All except ε Tau (vB 70) were previously detected by the *Einstein Observatory* (Stern et al. 1981; Micela et al. 1988); ε Tau was detected in the preliminary RASS study (Stern et al. 1992), and at a higher level of significance with a more accurate flux by Collura et al. (1993) in a *ROSAT* pointed observation. In the completed RASS observations, we now detect ε Tau at ML = 9.1 and a count rate of 0.015 ± 0.007 counts s^{-1}, compared to our preliminary estimate of ≈0.02 counts s^{-1}. Both rates are internally consistent and in agreement with the count rate found by Collura et al. (1993).

In the preliminary survey of Stern et al. (1992), we reported that δ Tau (vB41), which *had* been detected in the original Stern et al. (1981) Hyades survey, was not detected by *ROSAT*. However, with the increased exposure time of the completed RASS observations, we now report a detection near threshold

TABLE 2

REID STARS DETECTED IN X-RAYS[a]

Star	α (J2000 Opt) h	m	s	δ °	′	″	Photometry V	B-V	ML Ratio	PSPC cts/sec	Δ pos (arcsec)	Notes
RE12	3	58	35.8	13	6	18.5	8.97	0.66	18.3	0.026 ±0.009	10.8	non-member (Reid 1993)
RE119	4	15	32.6	20	48	25.3	17.34	1.69	17.7	0.056 ±0.015	40.8	LP414-138
RE299	4	31	15.7	10	42	15.0	14.91	1.37	14.3	0.022 ±0.008	4.0	
RE391	4	39	51.5	19	39	33.9	16.38	1.90	10.1	0.016 ±0.007	7.7	

[a] Reid candidates not included in earlier proper-motion surveys.

(ML = 8.7) at 0.02 ± 0.009 counts s^{-1}. This detection, as well, is in agreement with our preliminary upper limit. We will discuss more thoroughly the issue of long-term variability among the Hyades in § 8.

5.5. *Detections of Reid Candidates*

Although there are over 180 new Hyades candidates in the Reid (1992) proper motion survey near the cluster center, only four have been detected in the RASS data; these X-ray detections are presented in Table 2. The fact that most of the faint Reid proper motion stars are not detected is not surprising, given the X-ray luminosity function of M dwarfs in the cluster (see § 6) and the survey sensitivity limit. In addition, a number of the Reid (1992) candidates have subsequently been rejected by Reid (1993) on the basis of CCD photometry. Since radial velocity measurements for such faint stars are presently unavailable, some unknown additional fraction of these stars are likely to be nonmembers (as are a number of the fainter stars in our 440 member reference sample that have been confirmed by proper motions and photometry only). This will also lower the detection rate.

5.6. *Detections of Hyades Candidates Rejected as Members*

In Table 3 we provide a list of those stars in our large (1100+) catalog which have previously been rejected as Hyades members by photometry or radial velocity studies, but which were detected above our ML = 8 threshold in X-rays. We briefly discuss those objects which are brighter than 0.1 PSPC counts s^{-1}. VA 771 and BD +26°730 (V833 Tau) are short-period BY Dra binaries rejected as Hyades members on the basis of discordant radial velocities (Griffin et al. 1988). GH 8-2B is a white dwarf, but its X-ray flux is suspect, as it is confused with V833 Tau; vB 61 is a binary resolved by occultation but also rejected on the basis of its radial velocity. VA 247 is a dM star rejected by Hanson (1975) on the basis of proper motions, and LP 413−19 is rejected by Griffin et al. (1988) on the basis of radial velocity. We also note the much weaker source, GH 7−178, which was detected in a 40 ks *ROSAT* PSPC pointing by Stern et al. (1994).

Because of the relatively high (>40%) detection rate for the 440 member reference sample, and the relatively low (~3%) detection rate for the rejected Hyades candidates, it may be worth individually reexamining the membership status of those Hyads rejected only by, e.g., proper motion or photometry. The presence of the short-period binaries in Table 3 can easily be explained because of their enhanced activity. As for the remaining objects, radial velocity measurements are usually an excellent cluster membership indicator, but proper motion probabilities are inherently less reliable; hence, a few of the fainter stars in this table may, in fact, be cluster members.

TABLE 3

NONMEMBERS IN OPTICAL CATALOG DETECTED IN X-RAYS

Star	α (J2000 Opt) h	m	s	δ °	′	″	Photometry V	B-V	Binary[a] Codes	ML Ratio	PSPC cts/sec	Δ pos (arcsec)
L3	3	30	30.3	20	5	54.5	10.78	1.39		8.5	0.019 ±0.008	11.7
LP413-19	3	37	33.4	17	51	17.9	13.29	1.54		88.1	0.145 ±0.022	24.0
vB135	3	43	54.3	3	26	45.1	8.99	0.87		11.9	0.034 ±0.012	33.2
GH8-1	4	14	53.4	27	45	33.4	12.65	1.57		11.2	0.038 ±0.013	5.3
GH7-152	4	17	50.6	18	28	30.8	13.88	1.57		22.9	0.037 ±0.011	20.7
GH7-178	4	22	30.3	15	13	11.9	14.64	0.84		32.2	0.026 ±0.008	24.0
VA247	4	22	39.7	15	3	45.8	15.47	0.95		62.2	0.129 ±0.020	0.5
vB61	4	25	57.5	5	9	3.6	7.38	0.51		69.2	0.112 ±0.019	18.7
GH8-46	4	29	54.2	27	38	27.5				18.4	0.023 ±0.008	58.7
VA751	4	34	42.2	17	44	55.0	7.75	0.65		13.4	0.035 ±0.012	32.0
VA771	4	35	33.9	12	6	2.0	8.90	0.58	GR	203.7	0.224 ±0.025	6.1
vB184	4	36	0.1	16	32	26.7	10.83	1.26	UW	11.5	0.023 ±0.009	28.3
GH8-2B	4	36	44.9	27	9	53.7	15.94	0.65		845.2	0.820 ±0.044	0.3
V833 Tau	4	36	47.9	27	7	59.5	8.42	1.12		4749.5	2.613 ±0.076	3.7
LP415-1644	4	37	21.8	19	21	17.1	14.65	1.75		38.2	0.067 ±0.015	11.3
LP476-612	4	47	37.4	10	13	58.5	14.90			12.8	0.031 ±0.011	47.4
vB165	4	49	48.5	23	23	41.8	8.52	0.63		26.6	0.054 ±0.013	20.6
BD18:742	4	51	12.8	18	52	0.4	10.40	0.69		63.0	0.060 ±0.012	21.0
vB152	5	10	0.6	27	38	39.0	9.23	0.93		12.7	0.030 ±0.011	4.9
AK7-1312	5	11	59.9	20	7	1.9	10.92	0.91		11.8	0.015 ±0.007	22.7

[a] See notes to Table 1 for binary codes.

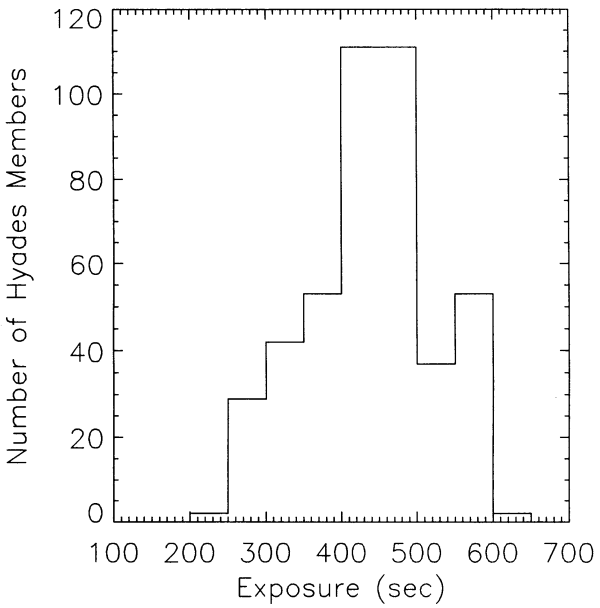

FIG. 7.—Distribution of survey exposure times for Hyades members (bin width = 50 s).

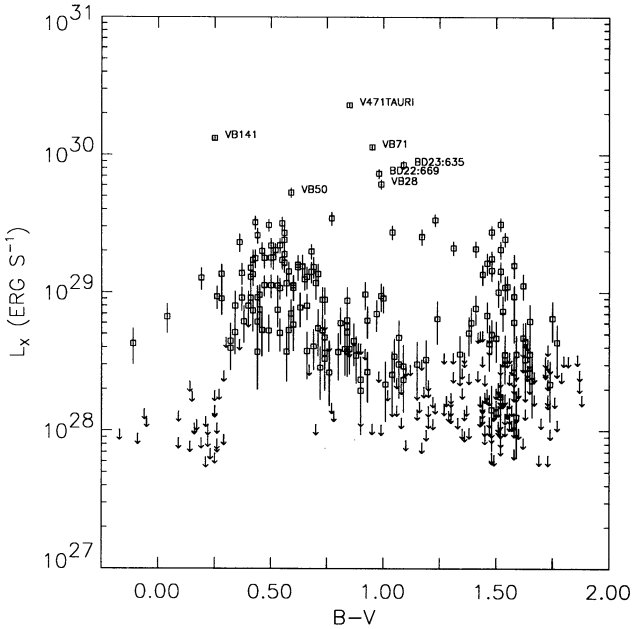

FIG. 8.—L_x vs. $B-V$ for detections (*boxes*) and upper limits (*arrows*). Error bars of 1 σ are shown for the detections. Brightest X-ray objects are labeled. L_x is calculated using an assumed distance of 45 pc for all stars. (Note that $B-V$ color is unreliable at values $\gtrsim 1.5$).

6. X-RAY FLUXES AND LUMINOSITIES

6.1. *Exposure Coverage and X-Ray Luminosity Limits*

Although the RASS survey provides complete coverage of the Hyades region, the limiting detectable flux varies because of the differences in net exposure time at individual sky locations and variations in the sky background (detector internal background variations produce a much smaller effect). The net exposure time ranges from $\approx$200–600 s, and the distribution is peaked at around 400 s (see Fig. 7). Consequently, the limiting PSPC count rate for detection ranges from $\approx$0.01–0.02 counts s^{-1}. Adopting for the present the conversion factor of 6.0×10^{-12} ergs cm^{-2} counts^{-1} (Stern et al. 1992, 1994; see also § 8), this corresponds to $\approx 0.6\text{–}1.2 \times 10^{-13}$ ergs cm^{-2} s^{-1} in the 0.1–1.8 keV band. This in turn corresponds to a limiting L_x of $\approx 1.5\text{–}3 \times 10^{28}$ ergs s^{-1} at the Hyades distance (45 pc), comparable to, but slightly better than, the sensitivity limit for a typical 2000 s *Einstein* IPC pointing in the 0.2–4.0 keV band.

6.2. *X-Ray Luminosity Functions*

In Figure 8 we plot the X-ray luminosities versus $B-V$ color for the detected and undetected Hyads, and in Figure 9 we plot the X-ray upper limits for the undetected cluster members from our final optical sample. We have determined the detection rates for Hyades members as a function of spectral type and luminosity class. These results are given in Table 4. We note in particular the very high ($\gtrsim$90%) detection rate for late F–G dwarfs.

We have computed the X-ray luminosity function as a function of $B-V$ color according to the classifications indicated in Table 4 and using methods appropriate for data which include upper limits (Feigelson & Nelson 1985; Schmitt 1985). We performed our computations using the ASURV Version 1.2 software package.[2] We caution, however, that except for the F–G stars, where the detection rate is over 90%, the ASURV calculations of the means and quartiles depend upon the assumption that the upper limits to the data have the same statistical distribution as the detected sources (Feigelson & Nelson 1985). However, for the Hyades RASS data, the objects with upper limits tend to be the intrinsically faintest objects, although this is mitigated somewhat by the variation in exposure times across the survey region. Hence, the means may be biased in some indeterminate fashion. We note that this also applies to the case of the Micela et al. (1988) survey, although

[2] As implemented by T. Isobe, M. LaValley, and E. Feigelson, Pennsylvania State University.

TABLE 4

SURVEY DETECTIONS BY $B-V$ COLOR[a]

Sp Type B-V	K0 III	WD (-0.2–0.3)	A-F (0.0–0.49)	G (0.5–0.79)	K (0.8–1.44)	M (1.45–2.0+)	M(V>15) (No B-V)	Total
Detected	4	1	41	51	44	42	4	187
Cataloged	4	10	63	57	110	147	49	440
Fraction	1.0	0.1	0.65	0.89	0.40	0.29	0.08	0.43
$< logL_x >$	29.2±0.4		28.59±0.08	28.92±0.05	28.30±0.05	28.12±0.04		28.29±0.03

[a] See § 2 for optical catalog selection.

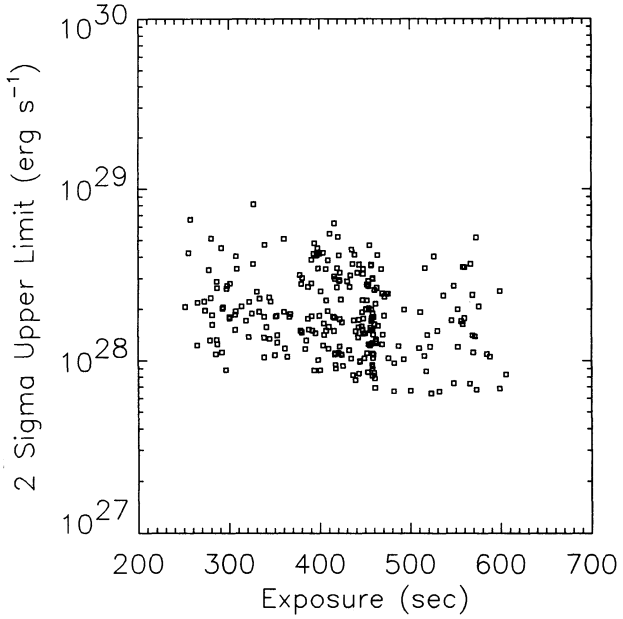

FIG. 9.—Upper limits vs. exposure times for undetected Hyads

in the latter case, variations in effective exposure time within each IPC field are also a mitigating factor. These biases mostly affect the luminosity functions for K and M stars (where the detection rate is lower), and to a lesser extent the luminosity functions for the F and G stars, where our detection rate is very high.

7. THE INFLUENCE OF BINARY SYSTEMS ON THE X-RAY LUMINOSITY FUNCTION

In Stern et al. (1992) we noted that, on the basis of the preliminary RASS results, X-ray–emitting Hyades binaries, especially those in short-period (< 10 day) binary systems, had significantly higher X-ray luminosities for their main-sequence spectral type than did ostensibly single systems. Now that the RASS study is complete, we may make a more thorough study of the influence of binary membership on our results. Our study is limited, especially at the faint end, by the observational difficulties in obtaining radial velocities for faint stars. Our primary compendium of spectroscopic binary information comes from the work of Griffin et al. (1988) and the many references cited therein. Griffin et al. performed a radial velocity survey of nearly all the probable or possible Hyads in the magnitude range $6 \lesssim V \lesssim 14$. In addition, Griffin (1993, private communication) has made available additional information regarding spectroscopic binaries whose orbital periods were determined after the publication of the Griffin et al. (1988) paper (for the most part, these are long-period systems). For brighter stars, we used the compendium of Batten, Fletcher, & McCarthy (1989) for spectroscopic binary references. A number of the stars in the Hyades are known visual or photometric binaries, or have been discovered to be binaries using lunar occultation measurements (see binary column and notes in Table 1). This group includes a number of stars fainter than the magnitude range covered by Griffin et al. (1988).

For the purposes of our binary study, we retained the grouping of Table 4: A–F stars, G stars, K stars, and M stars. We then divided each group into three samples: (1) single stars, (2) spectroscopic binaries, and (3) all other binaries. We again used the ASURV 1.2 software to compute cumulative X-ray luminosity functions for each group and the three samples within each group. The results of this analysis are shown as cumulative X-ray luminosity distributions in Figure 10. In one or two of the subsamples, e.g., A–F or M spectroscopic binaries, the numbers involved are small. However, it is quite clear that there is a striking divergence between the binary/single X-ray luminosity functions for the K stars, and possibly some difference for the M stars, unlike that for the F8–G5 stars, where there are few differences among the three samples. We point out that the case of the K star dichotomy was first demonstrated in the pointed *ROSAT* Hyades sample of Pye et al. (1994). Our results, with a much larger sample (110 vs. 17 stars), confirm their result that binaries of *any* type have a significantly different X-ray luminosity function than single stars for the K dwarfs, resulting in nearly an order of magnitude increase in the mean L_x for binary versus single stars. Formal applications of the Gehan, Logrank, Peto-Peto, and Peto-Prentice two-sample tests available in ASURV 1.2 yield $P < 10^{-4}$ that the binary and single K star samples come from the same distribution. This holds true for comparisons between single K stars and each of the two binary samples, although the total number of binaries (32) is dominated by spectroscopic binaries (SBs) with long (> 10 day) periods, and the number of "other" binaries is only seven. The M stars also exhibit this single/binary dichotomy, although in this case, the total number of confirmed binaries of all types amounts only to nine objects. The formal probabilities from the two-sample tests also yield an extremely low probability ($< 10^{-4}$) that the M star single and spectroscopic binary populations are the same, and a probability of < 0.02 that the samples for the single M stars and other M star binaries are the same. In contrast, with nearly equal numbers of single and binary stars, the F8–G5 single and binary X-ray luminosity functions are quite similar to each other: the probability that the single and spectroscopic binary G stars have the same distribution is $\approx$0.04–0.12, only marginally statistically significant, and $P \approx 0.15$–0.20 for the single G and other G binaries, a null result. These formal quantitative results are qualitatively apparent in Figure 10.

To further investigate the influence of binaries, we have studied the relationship between X-ray emission and binary period. In Figure 11 we plot L_x versus P_{bin} for all the SBs in the sample with determined periods, and the same for L_x/L_{bol} in Figure 12. Next, we divided the sample into color groups with $B-V < 0.6$ and > 0.6, the approximate color at which strong rotational braking is known to occur (Kawaler 1989). Stars in the Pleiades, for example, also show a dichotomy between these color groups in rotation-dependent activity and the lack thereof (Stauffer et al. 1994). Plots for L_x/L_{bol} versus P_{bin} for the two groups are shown in Figures 13*a* and 13*b*. These plots clearly demonstrate that for periods $\lesssim$10 days, the redder stars show a strong dependence upon binary period, while the bluer stars do not (vB 190 is anomalous because it has a rapidly rotating (3.66 day) component in the system, although it is a long-period binary as well). The transitional period of $\sim$10 days is in excellent agreement with the value of $\sim$8 days below which the orbital and rotational period of binaries are expected to become synchronous (Zahn & Bouchet 1989). Hence, the issues of rotational and binary influences on the X-ray luminosity distributions for the late type stars in the Hyades are tightly intertwined.

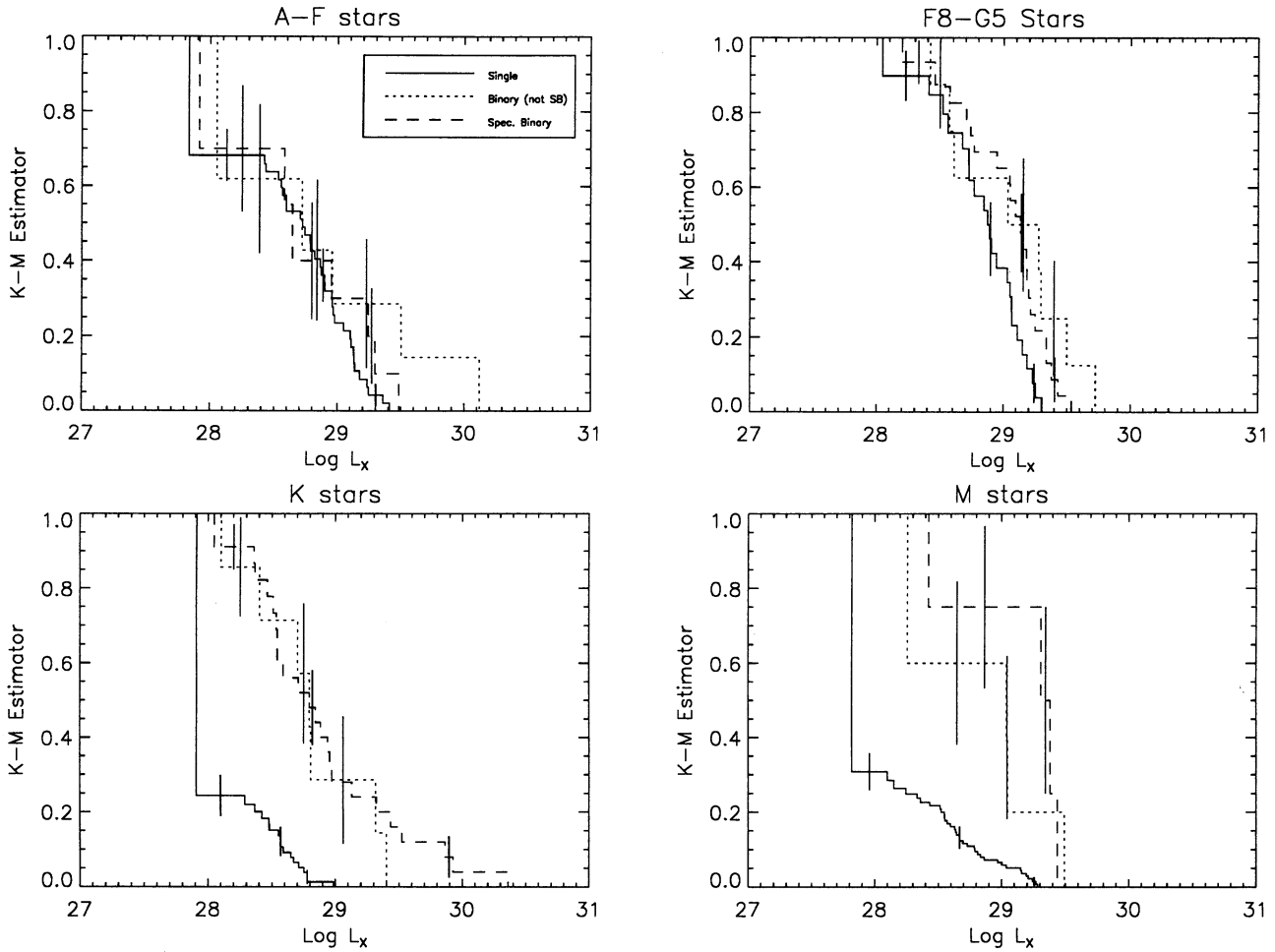

FIG. 10.—Cumulative X-ray luminosity functions for single (*solid line*), spectroscopic binary (*dashed line*), and other binary (*dotted line*) in the Hyades sample. (*a*) A–early F stars; (*b*) F8–G5 (solar type) stars; (*c*) K stars; and (*d*) M stars. Representative error bars are shown.

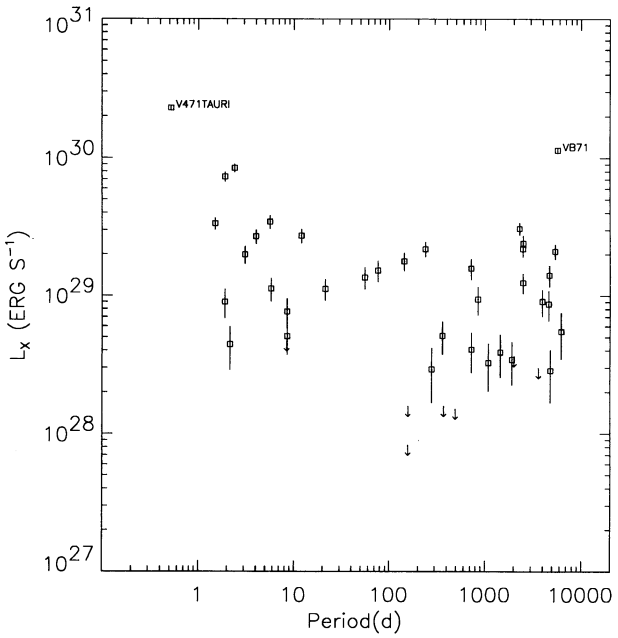

FIG. 11.—L_x vs. binary period for all spectroscopic binaries with determined periods in Hyades sample. Upper limits are indicated by arrows.

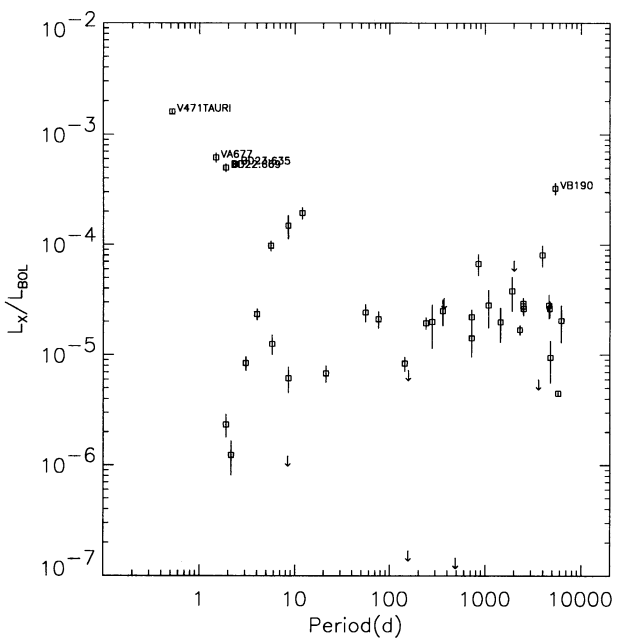

FIG. 12.—L_x/L_{bol} vs. binary period. See discussion in text.

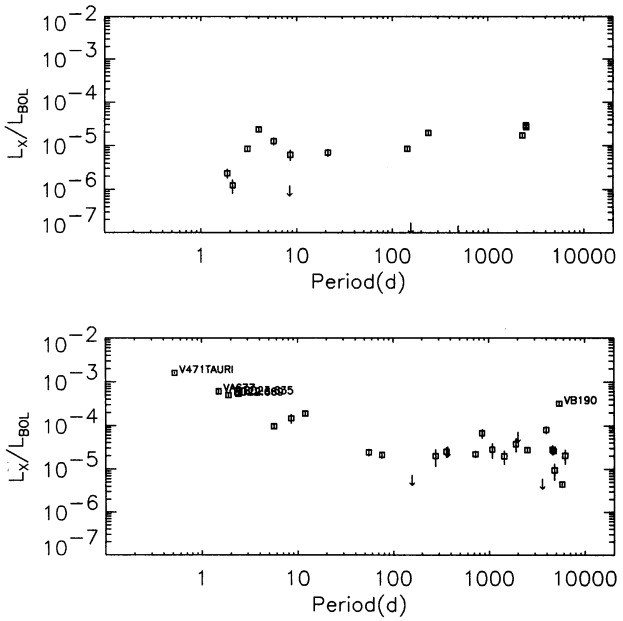

FIG. 13.—L_x/L_{bol} vs. binary period for (*a*) $B-V < 0.6$, (*b*) $B-V > 0.6$

8. *Einstein-ROSAT Comparison*

The comparison between the completed RASS Hyades survey and the older *Einstein* Hyades survey affords us the best opportunity to date for a study of the long-term X-ray variability in cool stars. By their very nature, the RASS data include either detections or upper limits for all the 127 objects (66 detections) in Micela et al. (1988). Since the epoch of the *Einstein* observations ranges from 1979–1981, and the Hyades region was scanned by *ROSAT* in 1990 August and 1991 February, our baseline is roughly a decade.

In Figure 14 we show a plot of the Hyades PSPC count rates for the *ROSAT* survey versus the *Einstein* IPC count rates from Micela et al. (1988) for those sources with detections in both surveys and for those sources with upper limits in one or both surveys that deviate more than a factor of 2 from the nominal conversion between PSPC and IPC counts. This nominal conversion factor is shown as a dotted line in the figure, with dashed lines on either side indicating bounds of a factor of 2 either way. In addition, we have labeled in the figure those objects with significant ($>2.5\ \sigma$) variability between the *Einstein* and *ROSAT* eras. The variation in vB 22 is easily explained, since it is a BY Dra system which flared in one of the *Einstein* observations (Stern, Underwood, & Antiochos 1983): Micela et al. (1988) reported the flaring X-ray flux. VA 334, VA 763, and LP 357−4 (Hz 2411) are all dM stars: Hz 2411 is a well-known flare star projected against the Pleiades (see, e.g., Stauffer et al. 1994). The remaining stars which exhibit long-term variability include three of the four Hyades giants (the fourth was not observed by *Einstein*). These are vB 71 (θ^1 Tau), vB 28 (γ Tau), and vB 41 (δ Tau). Note that both vB 71 and vB 28 are significantly (~1.5–2 times) brighter in the RASS data, and vB 41 is significantly dimmer (§ 5.4). The remaining objects all appear to vary no more than a factor of 2 over the decade-long interval; we would like to note, however, that we ascribe most of the dispersion in Figure 14 to variability between the *Einstein* and *ROSAT* measurements rather than simply to measurement errors, although the precise level of such long-term variability is quite difficult to establish in individual cases.

To verify the above results regarding long-term X-ray variability, it is instructive to compare the X-ray luminosity distributions for the RASS data and the *Einstein* data: if the cross-calibration between the IPC and PSPC is correct, then the means of the L_x distributions for a given class of stars should remain the same, even if there is long-term variability for individual objects. We chose to study the L_x distributions of the F8–G5 stars, for which our detection rate is ≈90% (51/57 objects detected), with a similar rate (but considerably fewer stars) for the Micela et al. (1988) survey (17/19 detected). The $\langle \log L_x \rangle$ for the RASS Hyades F8–G5 sample is 28.92 ± 0.05. This compares to 29.16 (+0.05, −0.07) for the Micela et al. (1988) *Einstein* sample. Is this a significant difference? Based upon the quoted errors in both cases, it is statistically significant, and somewhat of concern, since it might indicate up to a factor of 2 error in the cross-calibration of the PSPC and IPC. However, Stern et al. (1994) have demonstrated that, based upon model fits of PSPC pulse-height spectra for a representative sample of Hyades stars, the conversion factor from *ROSAT* PSPC counts to flux should be accurate to ~10%. To further investigate this apparent inconsistency, we restricted the RASS Hyades sample to *only those 19 stars* that were included in the earlier Micela et al. sample. The ASURV results in this case yielded a $\langle \log L_x \rangle$ of 29.15 ± 0.05 for the restricted RASS sample, virtually identical to the result obtained a decade earlier for the same group of stars by Micela et al. (1988). All the two-sample tests comparing cumulative distributions in ASURV 1.2 (e.g., Gehan, Logrank, Peto-Peto, Peto-Prentice: see references in ASURV documentation) yield a probability of ≈40% that these two samples are drawn from the same parent population.

What, then, do these results suggest? It is clear that cross-calibration between the two X-ray instruments is not an issue. However, it is possible that the *pointed* nature of the Micela et

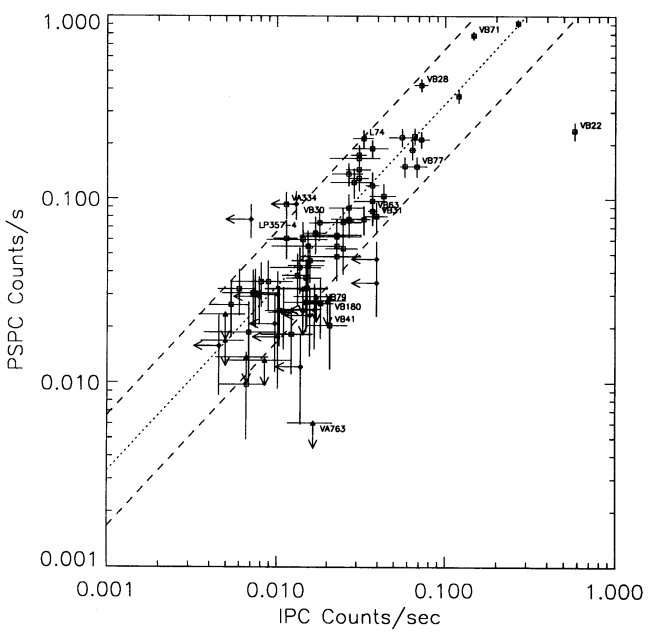

FIG. 14.—PSPC vs. IPC count rates for stars in both Micela et al. (1988) study and present RASS results. Dotted line represents the nominal PSPC/IPC conversion factor for unabsorbed coronal sources (see text). Dashed lines represent deviations of a factor of 2 from the nominal conversion factor. 1 σ count rate uncertainties are shown (arrows indicate upper limits).

al. (1988) survey may have introduced a subtle bias in the optical observational sample. In particular, since most of the G stars in the Micela et al. (1988) sample were originally observed in the Stern et al. (1981) survey of the central Hyades region ($\approx 5° \times 5°$), the *Einstein* results are characteristic of the cluster center, while the RASS results encompass the entire angular diameter of the cluster. We have searched for some systematic difference between the two samples in V, $B-V$, and individual distance, but we have found nothing statistically significant: the RASS sample is slightly redder ($\langle B-V \rangle$ of 0.62 vs. 0.64, but with a standard deviation for both samples of about 0.08), for example, but this should hardly cause a factor of 2 difference in L_x.

We also divided the RASS G star sample having intermediate (300–500 s) survey exposure times into two nearly equal (20 vs. 19) groups representing stars detected in the "inner" and "outer" Hyades regions. In this case, we also find no significant difference in the mean L_x. Thus, some sort of X-ray luminosity "segregation" in the F8–G5 star population appears to be ruled out (there is a known difference in the radial distributions of, say, the M stars vs. the G stars in the cluster; see Reid 1992). A variation in the binary incidence could be a possibility, but both samples have about 50% binaries, and if anything, the RASS sample has a higher proportion of short-period ($P < 10$ days) binaries than the *Einstein* sample (four vs. one). Also, in the previous section we demonstrated that the cumulative X-ray luminosity distributions of the single and binary G stars are quite similar, unlike those for the K and M stars. Another check we performed was to remove the anomalously X-ray bright G star vB 50 (BD +14°693) from both samples: this had a minor effect on the derived L_x distribution, and the two-sample tests still indicated that there was <5% probability that the RASS and Micela et al. samples came from the same population.

We also investigated the possibility that the RASS optical sample is contaminated by a few nonmembers incorrectly associated with the cluster by other researchers. From our original sample of 57 objects, we excluded 14 stars which were not included in the radial velocity measurements of Griffin et al. (1988) (the other 43 F8–G5 stars are confirmed members by photometry, proper motion, and radial velocity in the Griffin et al. study). Using ASURV, we derive $\langle \log L_X \rangle = 28.97 \pm 0.05$, which is the same result as that given in Table 4 within errors, but not in agreement with the Micela et al. (1988) result. Thus, we have no convincing explanation of why the characteristics of the two samples should differ other than the possibility that the small sample size (19 stars) of the Micela et al. (1988) sample is somehow affecting the comparison.

9. DISCUSSION

9.1. *X-Ray Activity, Stellar Mass, Rotation, and the Influence of Binary Systems*

By nearly tripling the number of X-ray detected Hyads, as well as providing upper limits to the X-ray flux for all optically identified cluster members (brighter than $V \sim 16$), the RASS results permit us a much clearer picture of the Hyades X-ray luminosity function than was possible from *Einstein*. In particular, the L_x distribution as a function of color (i.e., mass) along the main sequence, given in Figure 8, may be interpreted as a combination of a few basic factors which depend upon mass, binary influence, and, most probably, stellar rotation.

The paucity of A and early F star detections ($B-V < 0.3$) is not surprising and is consistent with the earlier Hyades surveys of Stern et al. (1981) and Micela et al. (1988) and with the results from other young clusters such as the Pleiades (Stauffer et al. 1994). The few exceptions have usually been attributed to faint binary companions (see Stauffer et al. 1994, and references therein), although recently a number of B stars have been detected as X-ray sources with no obvious late-type companion (e.g., Schmitt et al. 1993; Berghöfer & Schmitt 1994). Of the early-type Hyades detections in the present survey (seven in all with $B-V < 0.3$), three are unusual: the white dwarf EG 37 (VA 490), which has been discussed earlier and in Stern et al. (1992), the anomalously X-ray bright F0 star vB 141 (71 Tau), discussed in Stern et al. (1994), and the A5 short-period (1.89 days) and speckle binary 51 Tau (vB 24). In the latter two cases, the bright member of the binary or multiple system is unlikely to be the source of the X-ray emission.

Beginning roughly at $B-V \sim 0.35$, there is a clear rise in L_x, peaking at the late F–early G stars ($B-V \sim 0.55$). Discounting for the moment the unusually active binaries, and the bright giants vB 71 and vB 28, the dispersion in L_x is relatively narrow (about 1 order of magnitude), and systematically declining until we reach $B-V \sim 1.4$–1.5, i.e., late K or early M spectral type. At that point, the envelope of maximum L_x begins a second rise, with a few M dwarfs nearly as bright in X-rays as the brightest G dwarfs. As we have seen in § 7, a number of the X-ray bright M dwarfs are known binaries, and a number of as-yet undiscovered faint binaries could be influencing the distribution of the X-ray luminosity function as well. The M dwarf luminosity function, as determined in Pye et al. (1994) using deep *ROSAT* pointings, extends below our survey limit to at least $\log L_x = 27.4$, demonstrating a factor of at least 100 spread in the X-ray luminosity function for the M dwarfs, as noted by Stern et al. (1994). Another way of looking at the variation of X-ray emission among stars of different spectral type in the cluster is to examine the ratio of X-ray to bolometric luminosity (Fig. 15). Here two of the giants (vB 28 = γ and vB 71 = θ^1 Tau) stand out, as again vB 141 for

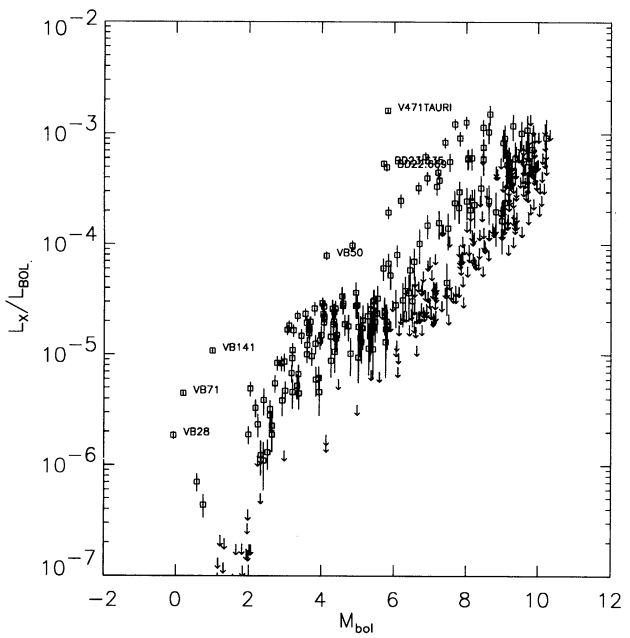

FIG. 15.—L_x/L_{bol} vs. bolometric magnitude. vB 28 and vB 71 are Hyades giants.

the most luminous stars. The binary sequence is again apparent for the fainter stars until $M_{bol} \approx 9$, where the phenomenon of "saturation" (e.g., Fleming et al. 1993) limits L_x/L_{bol} to $\lesssim 10^{-3}$.

How are these results related to current ideas regarding X-ray activity and stellar ages, mass, and rotation? In fact, the Hyades X-ray results are consistent with our rapidly developing understanding of the angular momentum evolution of late-type stars in open clusters (see review by Stauffer 1995). In this picture, stars are born with varying degrees of angular momentum at each spectral type. Edwards et al. (1993) have suggested that a major factor in determining the distribution of zero-age main sequence (ZAMS) rotation rates is the presence or absence of accretion disks in the pre–main-sequence (PMS) phase. Such disks serve as sinks for stellar angular momentum through, it is suggested, coupling of the stellar magnetic field or wind to the disk, which enforces corotation, thus preventing rapid spin-up of the star itself. Hence, stars without disks, or those stars with disks that dissipate rapidly, are expected to be faster rotators than stars with disks when they all arrive on the main sequence. Once on the main sequence, stars with the highest angular momentum spin down the most rapidly at each spectral class, with the spin-down time also being a function of mass: the lowest mass stars spin down more slowly than do the higher mass stars. By the age of the Hyades (700 Myr), the F, G, and early K stars have converged to a relatively narrow range of rotational velocities (the case for the later K stars is not yet proven due to observational limitations, although they must all be <10 km s^{-1}; see Stauffer, Hartmann, & Latham 1987). In contrast, the M star distribution of rotational velocities has not yet converged, resulting in a number of rapidly rotating M dwarfs, and, presumably, a number of slowly rotating M dwarfs by virtue of their PMS angular momentum (Stauffer et al. 1987). In the case of the Hyades, the transition from the converged G dwarfs to the unconverged M dwarfs is also likely reflected in the distribution of Hα emission as a function of color (Stauffer et al. 1991). The Hα results correlate quite well with the Hyades survey and pointing data (Stern et al. 1995). The only thing lacking at present to make this picture completely self-consistent is the availability of rotational period information for most of the late K and M dwarfs. Once this is obtained, the rotation-activity laws as a function of mass on the main sequence may be determined through comparison of the Pleiades, Hyades, and other young open clusters.

Complicating this picture is, of course, the influence of binary companions. This influence is most apparent for the short-period BY Dra systems present in the Hyades K star population (the most prominent examples are BD +22°669, BD +23°635, and VA 677). Since the stars in these systems are rotating much more rapidly than other Hyades K stars, their X-ray emission is enhanced, as we would expect. It is also conceivable that a faint short period binary system may be "hidden" in the anomalously bright vB 141 system (see Stern et al. 1994).

This does not, however, explain the significant differences in the luminosity functions between even wide binaries and single stars for spectral types K (and possibly M) as seen by Pye et al. (1994) and in Figure 10. From a theoretical standpoint, binary systems are expected to partially clear out or even disrupt PMS circumstellar disks, depending upon the binary separation (see review by Mathieu 1994). Thus, if the regulation of stellar angular momentum in the PMS phase by disks is, in fact, occurring as suggested in Edwards et al. (1993), and if binaries tend to disrupt disks or at least modify disk inner structure, the rotational regulation of PMS binaries may be affected. Artymowicz & Lubow (1994), for example, have developed theoretical models which demonstrate how, after only tens of orbital periods, binary systems clear out a substantial inner region of any circumbinary disk. If the inner disk is so disrupted, this may in turn result in either a large percentage of ZAMS rapid rotators in binary systems, or possibly a different internal angular momentum distribution in the stars themselves, resulting in different angular momentum evolution histories once the stars reach the main sequence. Obviously such a scenario must also account for the differences between the G and the K star X-ray luminosity functions for single and binary systems. This may be the result of varying lifetimes for the disks themselves as a function of mass (Strom et al. 1989 found typical dissipation times for disks $\sim 3 \times 10^6$–10^7 yr), or a stronger coupling between disks and stars with deeper convective zones.

9.2. *Long-Term X-Ray Variability in the Hyades Cluster and Implications for Dynamo Theories*

One of the key results of the current RASS Hyades study is the lack of large (i.e., greater than a factor of 2) variability in the individual X-ray fluxes of Hyades members over a decade-long baseline. We consider it unlikely that all the coronally active cluster members have a similar activity cycle, or one which was rather close to that of the Sun, or one with a period that was some submultiple of the 10 yr baseline. We hence conclude that the intrinsic long-term X-ray variability of the Hyades stars must be significantly less than that observed over the Sun's activity cycle, since the soft X-ray output of the Sun changes from solar minimum to maximum by a factor of 20–200 in the 0.2–0.25 and 0.6–1.5 keV bands of the Solrad satellites (Kreplin 1970). Most of the long-term Solar cyclic variability is seen as the growth or disappearance of active regions; this is especially the case for the 0.6–1.5 keV band, which contains many of the Fe XVII–XVIII lines characteristic of active region temperatures. The *ROSAT* PSPC response has a peak at ≈ 1 keV; thus, it is quite sensitive to the presence of this line emission. We are therefore forced to conclude that there is an enormous difference in the nature of the activity cycles, if any, for the Hyades solar-type stars compared to the Sun.

One possibility is that, e.g., the Hyades G dwarfs have much longer activity cycles than the Sun. This is unlikely, given even rudimentary dynamo theories (e.g., Durney, de Young, & Roxburgh 1993, and references therein). These would predict *shorter* activity cycles for G stars in the Hyades, which are rotating on average, about a factor of 5 faster than the Sun (Radick et al. 1987). A more likely scenario is that the Hyades G dwarfs (and other Hyades main-sequence stars) have dynamos which are continually producing new active regions on the stellar disk, with an activity cycle that results in a relatively small change from stellar activity minimum to maximum, in contrast to that of the Sun. There is evidence for this hypothesis in long-term Ca II emission core monitoring: Baliunas et al. (1995) find that, in G0–K5 V field stars, young stars (<1 Gyr) exhibit high average levels of activity and only rarely display a smooth, cyclic variation. The older stars, in contrast, display more "solar-like" behavior with relatively smooth cycles and occasional Maunder-minimum phases of extremely low activity.

It is conceivable that the lack of a strong activity cycle is also related to two alternative dynamo mechanisms: i.e., the so-called shell or core/convection zone dynamo, and the small-scale turbulent dynamo discussed in Durney et al. (1993). In this work, the authors suggest that the large-scale solar-cycle magnetic field is produced at the radiative core/convection zone boundary of the Sun (and stars), while the entire convective zone produces a small-scale turbulent magnetic field. The small-scale field does not require rotation but generates magnetic flux faster if rotation is present. Durney et al. go on to suggest that the presence of rapidly rotating M dwarfs in the Hyades is the result of the absence of large-scale magnetic fields, because they are fully convective stars. Although this is not quite correct (the rapid rotators discussed in Stauffer et al. 1987 are not completely convective), it may well be true that the turbulent small-scale dynamo mechanism dominates in these objects. The lack of a large-scale field, according to Durney et al., would result in a small Alfvénic radius (the distance corresponding to equality of the kinetic and magnetic energies of the stellar plasmas). Since the angular momentum loss via magnetic braking is proportional to the square of the Alfvénic radius, the spin-down time would be increased.

For the case of the Hyades G stars, which have already spun down considerably from stars of Pleiades age (Radick et al. 1987; Stauffer 1994), the large-scale "shell" dynamo may be identified with the mechanism of more rapid spin-down, while the small-scale turbulent dynamo, enhanced by the still rapidly rotating (10 km s^{-1}) G stars, may be contributing a significant proportion (say $>50\%$) of the total magnetic flux generation. Only the large-scale field would then undergo cyclic variations; hence, even if the flux generation due to the large-scale field disappeared at one point in the cycle, the magnetic flux generation rate would decrease by only, say, a factor of 2. Since the rate of magnetic flux generation is directly related to the coronal heating rate, and thus the observed X-ray luminosity, this would be consistent with the relatively low level of long-term variability seen in the Hyades main-sequence stars. Another implication for this picture would be the almost complete lack of X-ray activity cycles in the most active M dwarfs: this prediction has yet to be observationally tested.

10. SUMMARY

Our extensive and spatially complete survey of the Hyades region with *ROSAT* provides the best picture to date of the overall X-ray activity for stars in this cluster. Out of our 440 member sample, we detect 187 stars, down to an X-ray luminosity of ~ 1–2×10^{28} ergs s^{-1}. Our *ROSAT* positions are excellent, with mean systematic offsets between optical and X-ray positions of $<10''$ and overall positional uncertainties of $<1'$ (at $\gtrsim 99\%$ confidence). Among the detected X-ray sources identified with Hyades members are the four Hyades giants and one single white dwarf. The anomalously bright X-ray sources for a given spectral type are generally binaries. An X-ray "main sequence" emerges for late-A to G main-sequence stars, but then the dispersion in L_x increases dramatically for the Hyades K and M stars. One of the causes of this increased dispersion is binary incidence; the other is likely to be rotation. A 10 yr comparison between the *Einstein* and *ROSAT* data shows limited long-term variability (generally within a factor of 2) for the Hyades main-sequence stars that were studied with both observatories. This suggests the lack of strong cyclic activity compared to the Sun, possibly indicating that small-scale, turbulent magnetic field generation is much more dominant in G and later type stars of Hyades age than the large-scale dynamo that accounts for most of the Sun's magnetic cycle.

The *ROSAT* project has been supported by the Bundesministerium für Forschung und Technologie (BMFT) and the Max-Planck-Gesellschaft (MPG). Further, we would like to thank R. Neuhäuser for much help in the early stages of learning EXSAS techniques and for useful discussions regarding the RASS data, and C. Rosso for doing the initial processing of the RASS fields. R. A. S. wishes to thank J. Trümper for and the *ROSAT*/MPE team for their kind hospitality during an extended visit to MPE/Garching. A number of researchers provided electronic versions of their Hyades catalogs: E. Weis, R. Hanson, H. Schwan, N. Reid, and R. Griffin. We thank C. Prosser and D. Latham for useful discussions regarding Hyades photometry and binary incidence, and S. Baliunas for discussions regarding stellar activity cycles. We are especially grateful to J. Stauffer for extensive discussions and a careful reading of the manuscript. This research has made use of the SIMBAD database, operated at CDS, Strasbourg, France. R. A. S. was supported in part by NASA contract NAS5-32070, NASA grant NAGW-2698, and by the Lockheed Independent Research Program.

REFERENCES

Artymowicz, P., & Lubow, S. 1994, ApJ, 421, 651
Artyukhina, N. M., & Khopolov, P. N. 1975, Trans. Gos. Astron. Inst. Sternberg, 46, No. 2, 57
———. 1976, Trans. Gos. Astron. Inst. Sternberg, 47, 105
Baliunas, S. L., et al. 1995, ApJ, 438, 269
Batten, A. H., Fletcher, J. M., & McCarthy, D. G. 1989, Publ. Dom. Astrophys. Obs. Victoria, 17, 1
Berghöfer, T., & Schmitt, J. H. M. M. 1994, A&A, 292, L5
Bryja, C., Jones, T. J., Humphreys, R. M., Lawrence, G., Pennington, R. L., & Zumachs, W. 1992, ApJ, 388, L23
Collura, A., Maggio, A., Micela, G., Sciortino, S., Harnden, F. R., Jr., & Rosner, R. 1993, ApJ, 416, 204
Cruddace, R. G., Hasinger, G. R., & Schmitt, J. H. M. M. 1988, in Proc. ESO Conf. on Large Astronomical Databases, ed. F. Murtagh (Garching: ESO), 177
Durney, B. R., De Young, D. S., & Roxburgh, I. W. 1993, Sol. Phys., 145, 207
Edwards, S., et al. 1993, AJ, 106, 372
Eggen, O. J. 1969, ApJ, 157, 287
Feigelson, E. D., & Nelson, P. I. 1985, ApJ, 293, 192
Fleming, T. A., Giampapa, M. S., Schmitt, J. H. M. M., and Bookbinder, S. A. 1993, ApJ, 410, 387
Freyberg, M. J. 1994, Ph.D. thesis, Ludwig-Maximilian Universität, München
Giclas, H. L., Burnham, R., Jr., & Thomas, N. G. 1962, Lowell Obs. Bull., No. 5, 257
Griffin, R. F. 1993, private communication
Griffin, R. F., Gunn, J. E., Zimmerman, B. A., & Griffin, R. E. M. 1988, AJ, 96, 172
Gunn, J. E., Griffin, R. F., Griffin, R. E. M., & Zimmerman, B. A. 1988, AJ, 96, 198
Hanson, R. B. 1975, AJ, 80, 379
Kawaler, S. D. 1989, ApJ, 343, L65
Kraft, R. P. 1965, ApJ, 142, 681
———. 1967, ApJ, 150, 551
Kreplin, R. W. 1970, Ann. Geophys., 26, 567
Leggett, S. K., & Hawkins, M. R. S. 1989, MNRAS, 238, 145
Luyten, W. J., Hill, G., & Morris, S. 1981, Proper Motion Survey with the 48-Inch Schmidt Telescope (Minneapolis: Univ. of Minnesota)
Mason, B. O., & McAlister, H. A., Hartkopf, W. I., & Bagnuolo, W. G. 1993, AJ, 105, 220
Mathieu, R. D. 1994, ARA&A, 32, 465
Micela, G., Sciortino, S., Vaiana, G. S., Schmitt, J. H. M. M., Stern, R. A., Harnden, F. R., Jr., & Rosner, R. 1988, ApJ, 325, 798
Morel, M., & Magnenat, P. 1978, A&AS, 34, 477
McClure, R. D. 1982, ApJ, 254, 606

Osvald, V. V. 1954, & Astron. Nach., 281, 193
Pels, G., Oort, J. H., & Pels-Kluyver, H. A. 1975, A&A, 43, 441
Pfeffermann, E., et al. 1986, Proc. SPIE, 733, 519
Pye, J. P., Hodgkin, S. T., Stern, R. A., & Stauffer, J. R. 1994, MNRAS, 266, 798
Radick, R., Thompson, D., Lockwood, G., Duncan, D., & Baggett, W. 1987, ApJ, 321, 459
Randich, S., & Schmitt, J. H. M. M. 1995, A&A, in press
Reid, I. N. 1992, MNRAS, 257, 257
———. 1993, MNRAS, 265, 785
Schmitt, J. H. M. M. 1985, ApJ, 293, 178
Schmitt, J. H. M. M., Zinnecker, H., Cruddace, R., & Harnden, F. R., Jr. 1993, ApJ, 402, L13
Schwan, H. 1991, A&A, 243, 386
Simon, T. 1992, in Seventh Cambridge Workshop on Cool Stars, Stellar Systems, and the Sun, ed. M. S. Giampapa & J. A. Bookbinder (ASP Conf. Series Vol. 26), 3
Skumanich, A. 1972, ApJ, 171, 565
Soderblom, D. R., & Mayor, M. 1993, AJ, 105, 226
Stauffer, J. R. 1982, AJ, 87, 899
———. 1995, in Proc. 8th Cambridge Cool Star Workshop, ed. J. P. Cauillaut (PASP conf. series), in press
Stauffer, J. R., Caillault, J. P., Gagne, M., Prosser, C. F., & Hartmann, L. W. 1994, ApJS, 91, 625
Stauffer, J. R., Giampapa, M. S., Herbst, W., Liebert, J., Hartmann, L. W., & Stern, R. A. 1991, ApJ, 374, 142
Stauffer, J. R., Hartmann, L. Z., & Latham, D. W. 1987, ApJ, 320, L51
Stefanik, R. P., & Latham, D. W. 1985, in Proc. IAU Colloq. 88, Stellar Radial Velocities, ed. A. G. D. Phillip & D. W. Latham (Schenectady: L. Davies), 213
Stern, R. A. 1984, in Cool Stars, Stellar Systems, and the Sun, ed. S. L. Baliunas & L. Hartmann (Berlin: Springer), 150
Stern, R. A., et al. 1995, in preparation
Stern, R. A., Schmitt, J. H. M. M., Pye, J. P., Stauffer, J. R., & Simon, T. 1994, ApJ, 427, 808
Stern, R. A., Schmitt, J. H. M. M., Rosso, C., Pye, J. P., Hodgkin, S., & Stauffer, J. R. 1992, ApJ, 399, L159
Stern, R. A., Underwood, J. H., & Antiochos, S. K. 1983, ApJ, 264, L55
Stern, R. A., Zolcinski, M.-C., Antiochos, S. K., & Underwood, J. H. 1981, ApJ, 249, 647
Strom, K. M., Strom, S. E., Edwards, S., Cabrit, S., & Skrutskie, M. F. 1989, AJ, 97, 1451
Trümper, J. 1983, Adv. Space Res., 2, No. 4, 241
Trümper, J., et al. 1991, Nature, 349, 579
Upgren, A. R. 1974, ApJ, 193, 359
Upgren, A. R., & Weis, E. W. 1977, AJ, 82, 978
Upgren, A. R., Weis, E. W., & Hanson, R. B. 1985, AJ, 90, 2039
van Altena, W. F. 1969, AJ, 74, 2
van Bueren, H. G. 1952, Bull. Astron. Inst. Netherlands, 11, 385
Voges, W. 1992, in Proc. European ISY Meeting Space Sciences with Particular Emphasis on High Energy Astrophysics, 222
Weis, E. W. 1983, PASP, 95, 29
Weis, E. W., DeLuca, E. E., & Upgren, A. R. 1979, PASP, 91, 766
Weis, E. W., & Hanson, R. B. 1988, AJ, 96, 148
Weis, E. W., & Upgren, A. R. 1982, PASP, 94, 475
Wilson, O. C. 1966, ApJ, 144, 695
Wilson, R. E. 1948, ApJ, 107, 119
Zahn, J.-P., & Bouchet, L. 1989, A&A, 223, 112
Zimmermann, H. U., Belloni, T., Izzo, C., Kahabka, P., & Schwentker, O. 1993, EXSAS User's Guide (MPE Report 244)